ELSEVIER

Stability of perovskite materials and devices

Weifei Fu [1,a], Antonio Gaetano Ricciardulli [1,b], Quinten A. Akkerman [2,3,c], Rohit Abraham John [2,3], Mohammad Mahdi Tavakoli [4], Stephanie Essig [5], Maksym V. Kovalenko [2,3,*], Michael Saliba [1,5,6,*]

[1] Institute of Materials Science, Technische Universität Darmstadt, Alarich-Weiss-Straße, Darmstadt, Germany
[2] Laboratory of Inorganic Chemistry, Department of Chemistry and Applied Biosciences, ETH Zürich, CH-8093 Zürich, Switzerland
[3] Laboratory for Thin Films and Photovoltaics, Empa – Swiss Federal Laboratories for Materials Science and Technology, CH-8600 Dübendorf, Switzerland
[4] Department of Electrical Engineering and Computer Science, Massachusetts Institute of Technology, Cambridge, MA 02139, USA
[5] Institute for Photovoltaics (ipv), University of Stuttgart, Pfaffenwaldring 47, 70569 Stuttgart, Germany
[6] Helmholtz Young Investigator Group FRONTRUNNER, IEK5-Photovoltaik, Forschungszentrum Jülich, 52425 Jülich, Germany

Due to the excellent optoelectronic properties, organic–inorganic perovskites have drawn much attention and have been applied in different electronics with remarkable performance. However, the poor stability creates a massive barrier for the commercialization of perovskite electronic devices. In this review, we discuss intrinsic and extrinsic factors causing instabilities of perovskites and perovskite devices such as solar cells, liquid crystal displays (LCDs), light emitting diodes (LEDs), ionizing radiation detectors, transistors, memristors and sensors. We further review the stabilization approaches, including composition engineering, adoption of lower dimensional compositions, quantum dots, interface engineering, defects engineering and so on.

Keywords: Halide perovskite; Optoelectronic devices; Degradation; Stabilization approaches

Introduction

Organic–inorganic perovskites with an ABX_3 structure, where A is Cs^+, methylammonium (MA^+) or formamidinium (FA^+), B is Sn^{2+} or Pb^{2+}, and X is Cl^-, Br^- or I^-, have been widely investigated for optoelectronic applications in recent years. The synergistic effects of the outstanding material properties, like tuneable optical bandgap [1–4], high absorption coefficient [5], long carrier diffusion length [6–8], low exciton binding energy [9], high oscillator strength [10], fast and efficient photoluminescence [11], and major device engineering developments [12–14] have led to unprecedented achievements in the field of optoelectronics. For example, the power conversion efficiency (PCE) of single-junction perovskite solar cells (PSCs) has achieved a certified value of 25.7% [15]. While the light-harvesting performance is already at the level of commercialization, the device stability still lags behind commercially available photovoltaic modules. Furthermore, the application of perovskites in other optoelectronics such as light emitting diodes (LEDs) [16], lasers [17], light sources [18], photodetectors [19–22], and liquid crystal displays (LCD) [23] also suffer from stability issues. The instability of halide perovskites is caused both by intrinsic and extrinsic factors. On the one hand, intrinsic instability originates from the perovskite material itself, like thermal, chemical and phase instabilities. Those performance-limiting mechanisms can be reduced by optimization of the perovskite materials with mixed cations or lower-dimensions [24–27]. On the other hand, extrinsic fac-

* Corresponding authors.
E-mail addresses: Kovalenko, M.V. (mvkovalenko@ethz.ch), Saliba, M. (michael.saliba@ipv.uni-stuttgart.de).
[a] Present address: State Key Laboratory of Silicon Materials, MOE Key Laboratory of Macromolecular Synthesis and Functionalization, International Research Center for X Polymers, Department of Polymer Science and Engineering, Zhejiang University, Hangzhou, China.
[b] Present address: Université de Strasbourg, CNRS, ISIS UMR 7006, Strasbourg, France.
[c] Present address: Lehrstuhl für Photonik und Optoelektronik, Nano-Institut München und Fakultät für Physik, Ludwig-Maximilians-Universität (LMU), Königinstr. 10, D-80539 München, Germany.

 https://doi.org/10.1016/j.mattod.2022.06.020

tors such as interfaces and electron/hole transport layers also significantly affect the stability of perovskites and thus the overall device [28–32]. To improve the stability of perovskite devices, both extrinsic and intrinsic degradation factors need to be considered.

This review addresses the intrinsic and extrinsic stability of perovskites, their origin, and possible mitigation strategies. Further, we introduce the stabilization methods for devices, including solar cells, LCDs, LEDs, ionizing radiation detectors, transistors, memristors and sensors. Finally, we provide a summary and outline the perspectives toward high performance and highly stable optoelectronics.

Stability

Thermal stability

Depending on the location and architecture of the solar module, temperature of the solar cell may rise up to 95 °C [33,34]. Hence, thermal stability represents one of the major concerns in the field of perovskites. The soft matter nature of methylammonium lead halides ($MAPbX_3$) triggers structural transformation under thermal stress, posing an obstacle [35]. Although the $MAPbI_3$ single crystal is stable up to 300 °C [36], significant changes already occur during annealing at 85 °C for the polycrystalline films due to the partially volatile MA species [37,38]. The material is also prone to degrade to PbI_2 under humidity and light [39]. Particularly, continuous exposure of $MAPbI_3$ at high temperatures meeting the International Standards (85 °C) leads to decomposition of perovskite into volatile gas species like CH_3I and NH_3, as well as reversible decomposition into CH_3NH_2, HI, I_2 and finally non-volatile Pb^0 as follows (Fig. 1a) [38]:

$$MAPbI_3(s) \overset{hvor\Delta}{\leftrightarrow} PbI_2(s) + Pb^0(s) + I_2(g) + CH_3NH_2(g) + CH_3I(g) + HI(g) + NH_3(g)$$

The stability of the $MAPbI_3$ can be improved by compositional engineering of A cations, introducing Br^- at X sites, grain boundary and surface passivation, and encapsulation [25,40]. The substitution of MA with larger species can hamper the loss of organic cation. For instance, FA-based perovskites exhibit enhanced thermal stability [3,41], and decompose at temperatures above 95 °C, leading to the formation of *sym*-triazine [42]. However, as we will discuss in the following section, pristine $FAPbI_3$ lacks structural (phase) stability at room temperature [43]. The above decomposition processes are not only triggered by heat, but also by prolonged UV light exposure, creating a serious problem for perovskite solar cells. Luckily, these thermal and UV triggered decomposition processes can be reduced by suitable encapsulation [37,38,44]. Other strategies to increase thermal stability include the use of inorganic cations such as Cs^+ [25]. Indeed, fully inorganic perovskites, like caesium lead halides, are thermally stable up to 580 °C [45] and show longer aging stability than $MAPbX_3$ [46]. With a bandgap of 1.73 eV, 0.22 eV wider than $MAPbI_3$, $CsPbI_3$ could be an ideal top cell candidate for tandem solar cells to further increase the device performance of silicon or perovskite solar cells. Compared to the mixed-halide perovskites, $CsPbI_3$ perovskites can deliberately avoid phase segregation, leading to its outstanding photostability. However it suffers from structural instability at room temperature where it exhibits a photoinactive yellow phase, as will be further discussed in the next section [47,48]. To overcome this problem, structurally and thermally stable perovskites have been found upon integration of mixed FA-Cs cations [1,25,49]. Double perovskites such as Cs_2SnI_6, Cs_2TiBr_6, $Cs_2AgBiBr_6$ are another type of inorganic halide perovskites which could achieve excellent phase and thermal stabilities [50–52]. They are less investigated compared to the ABX_3 type perovskites with much worse performance, for example the record efficiency of $Cs_2AgBiBr_6$ solar cell is only 3.11% [53] and more work should be conducted to improve their optoelectronic performance.

Phase stability

The investigation of structural stability is a critical issue for many applications. Despite the favourable optical bandgap and long-term thermal stability of perovskites like $FAPbI_3$ and $CsPbI_3$, the spontaneous transition from the cubic α to orthorhombic δ phase limits their practical use. To evaluate the parameters that influence the crystal phases, introducing tools to discriminate them is of primary importance. The Goldschmidt tolerance factor (t) is a geometrical consideration to predict which perovskite structure is preferentially formed, as suggested by the following formula [54]:

$$t = \frac{(R_A + R_X)}{\sqrt{2}(R_B + R_X)}$$

where R_A and R_B are the ionic radii of the A and B cations, respectively, and R_X is the radius of the anion X. Empirically, photoactive perovskite structures are formed in the range $0.8 < t < 1$. In contrast, non-perovskite structures occur for values below 0.8 and above 1, resulting in crystal structures with a lower-dimensional Pb-halide framework [55]. These lower-dimensional phases often consist of facet or face shared Pb-X octahedrons, not only increasing the bandgap of perovskites due to less orbital overlap, but also forming indirect bandgap materials, such as the orthorhombic "yellow" phase of δ-$CsPbI_3$ at room temperature. Thermally stable perovskites like $FAPbI_3$ and $CsPbI_3$ are borderline cases with tolerance factors at 1.0 and 0.8, respectively [56]. As a consequence, their black photoactive α-phases are thermodynamically unfavorable than the cubic phase at room temperature and will transform into the undesired photoinactive yellow δ-phases at room temperature (Fig. 1b) [57], moisture could catalyze the transformation [58]. To optimize the tolerance factor and enhance the stability of the α-phase, mixing $FAPbI_3$ with smaller cations e.g. MA, Cs^+, or Rb^+, has become an effective strategy in recent years [25,49,59]. Anion engineering with halides [43,60] or the pseudo-halide anions such as $HCOO^-$ [61], SCN^- [62] could also stabilize the α-phase $FAPbI_3$ with optimized tolerance factor and reduced lattice constant. Moreover, the incorporation of small amounts of bulky 2D perovskites, such as phenylethylammonium lead iodide (PEA_2PbI_4), is an alternative route to stabilize the α-phase of $FAPbI_3$ films by reduction in lattice constant showing enhanced radiative lifetimes [63,64]. PEA_2PbI_4 is formed at the grain boundaries of $FAPbI_3$, passivating the surface defects and preventing moisture-induced phase degradation. Further, a myriad of pathways towards phase stabilization has been explored by polyelemental mixing [65]. Recently, Bartel et al. introduced a new tolerance factor (τ) to predict the stability of the perovskite structure [66], which has the form.

$$\tau = \frac{R_X}{R_B} - n_A\left(n_A - \frac{R_A/R_B}{\ln(R_A/R_B)}\right)$$

where n_A is the oxidation state of A, and $\tau < 4.18$ indicates perovskite. A higher overall accuracy of 92% is achieved with τ compared to that

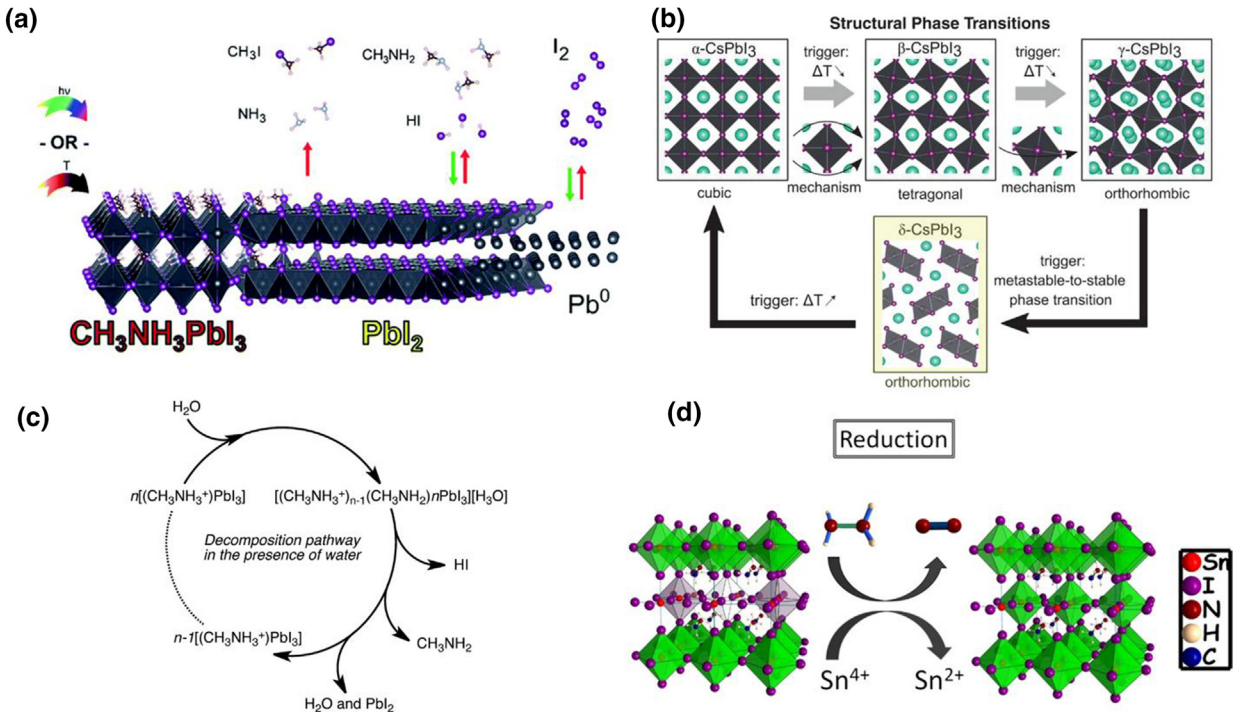

FIGURE 1

(a) $MAPbI_3$ photodecomposition and thermal degradation processes prompting irreversible decomposition into organic volatile gas species (CH_3I + NH_3), reversible decomposition (CH_3NH_2 + HI), and reversible generation of I_2 and non-volatile Pb^0 under illumination or mild heat conditions. Reproduced from Ref. [38] with permission from the Royal Society of Chemistry. (b) Crystal structure of the cubic, tetragonal and orthorhombic phases, and their relative phase transitions. From [57]. Reprinted with permission from AAAS. (c) Possible decomposition pathways of hybrid halide perovskites in the presence of water. Reprinted with permission from [69]. Copyright 2014 American Chemical Society. (d) Suggested mechanism of hydrazine vapor reaction with Sn-based perovskite materials. Reduction process: $2SnI_6^{2-} + N_2H_4 \rightarrow 2SnI_4^{2-} + N_2 + 4HI$. Reprinted with permission from [71]. Copyright 2017 American Chemical Society.

of 74% for the typical t. Nearly uniform performance across the five anions evaluated [oxides (92% accuracy), fluorides (92%), chlorides (90%), bromides (93%), and iodides (91%)] could be achieved with τ, while t performs considerably worse for compounds containing heavier halides [chlorides (51% accuracy), bromides (56%), and iodides (33%)] than for oxides (83%) and fluorides (83%). τ may be used to accelerate the discovery and design of state-of-the-art perovskite materials.

In contrast to chemical-based methods, phase stabilization of $FAPbI_3$ induced by strain engineering has been recently reported [67,68]. In the work of Chen et al., α-$FAPbI_3$ was epitaxially grown on a methylammonium lead chloride/bromide ($MAPbCl_{1.50}Br_{1.50}$) single crystalline substrate. The stabilization of the α-phase is generated by the synergistic effect of two factors: (1) the strong nature of ionic bonds between the epitaxial lattice and the substrate, which hinders the phase transition of the lattice; (2) the compressive strain (2.4%) that neutralizes the effect of the internal tensile strain responsible to the α-to-δ phase transition.

Chemical stability

The first perovskite material whose environmental stability has been extensile studied is $MAPbI_3$. It gained significant attention due to its relatively simple composition and easy fabrication by wet-chemical methods [5]. Perovskites tend to adsorb the atmospheric moisture because of their ionic characteristics of the constitutive chemical bonds; they subsequently react into hydrated compounds. For example, exposure of $MAPbI_3$ to water vapor results in the formation of $MAPbI_3{\cdot}H_2O$, followed by $(MA)_4PbI_6{\cdot}2H_2O$ upon longer exposure with water diffusion along the grain boundaries. Even though this process is reversible; excess water may result in irreversibly degrading the structure (Fig. 1c) [69,70] due to the subsequent formation of MAI and PbI_2.

Sn-based perovskites are of increasing interest due to the lower toxicity and narrower bandgaps compared to their Pb-based counterparts. However, they suffer from the facile oxidation of Sn^{2+} to Sn^{4+} destabilizing the perovskite structure, even negligible oxidation would lead to degenerate doping levels, making the semiconductor unsuited for most purposes [71,72]. Tin oxidation is predicted to be less likely in bulk $MASnI_3$ while it is energetically favoured at unpassivated perovskite surfaces [73]. Stabilizer or reducing chemicals, such as SnF_2-pyrazine complex [74], hydrazine vapor [71], ammonium hypophosphite [75], ascorbic acid [76], formamidine sulfonic acid [77], and tin powder [78,79] are efficient and necessary to inhibit the formation of Sn^{4+} defects (Fig. 1d).

Perovskite quantum dots (QDs) attract significant interest in recent years for PSC, LED, LCD applications due to their unique optical properties, such as tunable wavelength, narrow emission, and high photoluminescence quantum efficiency. However, due to the highly dynamic binding on the surface of perovskite QDs, the ligands are easily lost during the isolation and purification procedures, which makes it difficult to achieve long-term stability [27,80]. Hens et al. demonstrated that when a small amount of both oleic acid and oleylamine is added, the QDs can be puri-

fied, maintaining optical, colloidal, and material integrity due to the improved binding of the carboxylic acid [81]. Luther et al. developed a process to purify the QDs by using methyl acetate (MeOAc) to remove excess unreacted precursors and without full removal of the surface species to avoid agglomeration and conversion to the orthorhombic phase. Using this extraction procedure, QDs which are stable in the cubic phase for months with ambient storage are achieved [82]. On the other hand, appropriate surface capping ligands could efficiently reduce surface defects and suppress surface decomposition induced by oxygen and moisture. For example, Zhang et al. demonstrated that branched ligands (3-aminopropyl)triethoxysilane (APTES)-capped perovskite QDs show higher stability in protic solvents compared to the conventional QDs capped with straight-chain ligands. This is due to the strong steric hindrance and propensity for hydrolysis of APTES, which prevent protic solvent molecules from reaching and reacting with the core of QDs [83].

Ion migration

Ion migration in halide perovskite films has been attributed as the major causal factor for hysteretic behaviour in optoelectronic responses, unstable/transient behaviour and device degradation [84], evidenced by various spectroscopy techniques [85,86], electrical parameter analyses [87] and microscopy [88]. In halide perovskites, ions can hop across interstitials and defects, and the soft lattice of these materials facilitate easy diffusion across the crystal structure. As a result, this ionic transport gets naturally coupled with intrinsic electronic semiconductivity of perovskites, resulting in a mixed ionic-electronic conductor. The movement of ions in the bulk causes localized self-doping [88,89], making it challenging to monitor the energy level alignment with transport layers precisely. At the interfaces, the ions get blocked, but can alter the electronic properties of the interface or trigger electrochemical reactions, producing negative capacitance and irreversible degradation [90–94]. These affects are further accentuated under illumination and are the source for most of the undesirable device characteristics observed in photovoltaics, LCDs, LEDs, hard radiation detectors, transistors, etc. Detailed explanation on how these affect the device technologies, and notable mitigation strategies are discussed in the device-respective sections below.

Light stability

Light illumination may serve as an accelerator in the degradation process of perovskites. The excess of both holes and electrons generated by incident light or by current-injection from electrodes could reduce the activation energy for ion migration within perovskites, accelerating the degradation of perovskites [95]. $MAPbI_3$ films undergo rapid degradation when exposed to oxygen and light by photo-induced formation of highly reactive superoxide species. Perovskite films composed of small crystallites show higher yields of superoxide and lower stability. Ab initio simulations indicate that iodide vacancies are the preferred sites in mediating the photo-induced formation of superoxide species from oxygen. The film and device stability could be enhanced by passivation and interlayers which are able to remove electrons from the perovskite film before they can react with oxygen to form O_2^- [96,97]. Perovskite/transporting layers (TL) interfaces will also significantly affect the light stability of the perovskite optoelectronics. For example, devices incorporated with TiO_2 which is widely used in high performance PSCs degrade under UV light exposure due to the deep traps formed by the reaction of photo generated holes and oxygen absorbed at surface oxygen vacancies in TiO_2 [29,98]. Hard X-ray photoelectron spectroscopy (HAXPES) and impedance spectroscopy show accumulation of iodine and metallic lead in the vicinity of the perovskite-hole transporting layer (HTL) and perovskite-electron transporting layer (ETL) interfaces, respectively, accounting for highly damaged perovskite-TL interfaces during light-induced degradation (LID) [99].

The bandgaps of perovskites could easily be tuned by varying halide ratios (Cl/Br and Br/I) to satisfy the requirement of different kinds of optoelectronic applications in tandem solar cells [60], wavelength-tunable LEDs [100] and lasers [17]. However, the mixed-cation, mixed-halide perovskites suffer from halide redistribution which results in phase separation of I- and Br-rich domains under steady state illumination or with applied bias [101,102]. McGehee et al. firstly reported the reversible, light-induced transformations in $MAPb(Br_xI_{1-x})_3$. They found that light soaking causes a splitting of X-ray diffraction (XRD) peaks and a new red-shifted peak in photoluminescence spectra. These photo-induced changes are fully reversible after the materials are left for a few minutes in the dark [103]. Ginsberg et al. found that the unique combination of mobile halides, substantial electron–phonon coupling, and long-lived charge carriers is required for photoinduced phase separation. Decreasing defect concentrations to reduce vacancy-mediated halide migration or lowering electron–phonon coupling could significantly reduce photoinduced segregation [104]. Kuno et al. found that the driving force behind phase separation is the bandgap reduction of iodide-rich phases by using combined spectroscopic measurements and theoretical modelling. Their model also reveals that mixed halide perovskites can be stabilized against phase separation by deliberately engineering carrier diffusion lengths and injected carrier densities [105]. Phase segregation induced by light could be efficiently supressed by composition engineering, lower dimensional structures, device engineering which will be discussed in detail in the following sections.

Perovskite compositions and stabilization approaches

3D mixed cation perovskite

Many of the frequently highest performing ABX_3 perovskites use, for example, K, Rb, Cs, MA, or FA as cations, Pb, or Sn as metal ions, and Cl, Br, or I as halides (Fig. 2a) [65]. To induce preferable crystallization of the photoactive α-phase in FA-based perovskites, the incorporation of smaller cations with high dipole such as MA in $FAPbI_3$ has been a successful strategy [41,43,106,107]. Alternatively, the introduction of Cs^+ has been used to fine-tune the Goldschmidt tolerance factor of $FAPbI_3$, assisting the entropic stabilization of $FAPbI_3$ α-phase through the formation of Cs/FA mixed perovskite [49,56,108,109]. Indeed, the non-photoactive hexagonal δ-phase is energetically unfavourable upon cationic mixing [110]. Higher degrees of freedom towards both enhanced performance and stability can be achieved by using multiple cation formulations. Triple cation

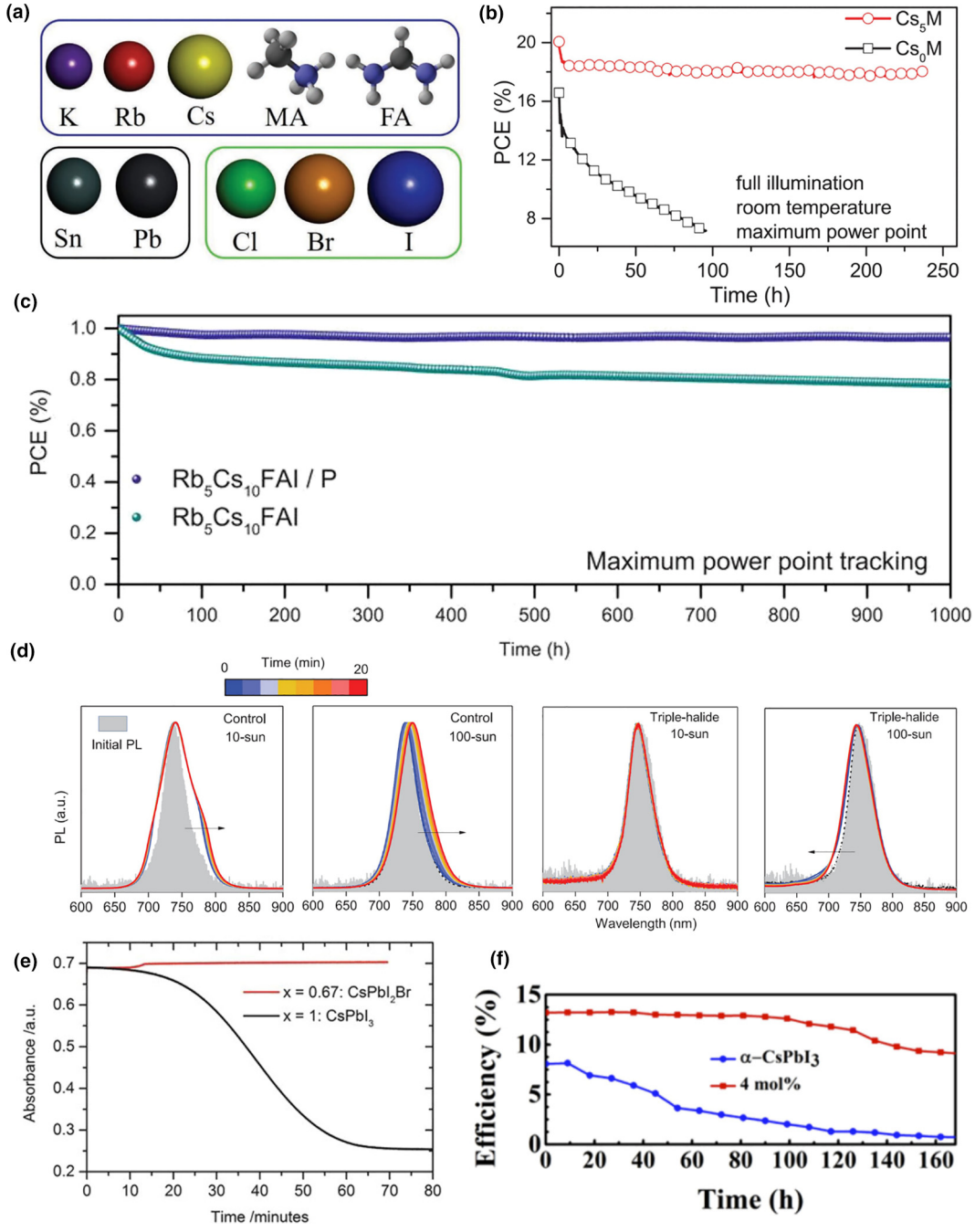

FIGURE 2

(a) Components reported in state-of-the-art perovskite solar cells (mainly aiming at 3D perovskites), i.e., A = [K, Rb, Cs, MA, FA], M = [Sn, Pb], X = [Cl, Br, I]. Reproduced with permission of [65]. Copyright 2018 John Wiley & Sons, Inc. (b) Aging for 250 h of a high performance $Cs_x(MA_{0.17}FA_{0.83})_{1-x}PbI_{2.49}Br_{0.51}$ (x = 0, 0.05) devices in a nitrogen atmosphere held at room temperature under constant illumination and maximum power point tracking. Reproduced from Ref. [25] with permission from the Royal Society of Chemistry. (c) Stability for the $Cs_{0.1}Rb_{0.05}FA_{0.85}PbI_3$ device without polymer layers (green curve) and with polymer-modification (blue curve) aged at room temperature after 1000 h of continuous maximum power point (MPP) tracking in a nitrogen atmosphere. From [111]. Reprinted with permission from AAAS. (d) PL spectra of 1.67-eV control perovskite films ($Cs_{25}Br_{20}$) and triple-halide perovskites ($Cs_{22}Br1_5 + Cl_3$) under 10-sun and 100-sun illumination for 20 min, respectively. From [60]. Reprinted with permission from AAAS. (e) Absorbance over time of thin films of $CsPbI_3$ and $CsPbI_2Br$, measured at 675 and 625 nm respectively, when exposed to a slow flow of air at 50% relative humidity (RH). Reproduced with permission of [112]. Copyright 2018 John Wiley & Sons, Inc. (f) PCE comparison of solar cells with pure α-$CsPbI_3$ and $CsPb_{0.96}Bi_{0.04}I_3$ layers upon air exposure. Reprinted with permission from [114]. Copyright 2017 American Chemical Society.

perovskite films containing Cs, MA and FA cations showed superior thermal stability and charge transport properties than traditional MA/FA mixtures, evidenced by minimum performance losses in aging tests (Fig. 2b) [25]. To further enforce the crystallization of the photoactive perovskite phase, Rb^+, which has an ionic radius slightly smaller (152 pm) than Cs^+ (167 pm), was successfully embedded in the Cs/FA/MA perovskite composition [59]. The resulting films showed exceptional material properties

and thermal stability. Saliba et al. further removed the thermally-unstable MA and fabricated the $Cs_{0.1}Rb_{0.05}FA_{0.85}PbI_3$ perovskite solar cells, which show high efficiency and high stability (Fig. 2c), providing an MA-free alternative [111]. McGehee et al. demonstrated that triple-halide alloys (chlorine, bromine, iodine) could suppress photoinduced phase segregation in wide–bandgap perovskites, needed for tandem applications with silicon solar cells. Photoluminescence (PL) studies showed a suppressed light-induced phase segregation in films even under 100-sun illumination and achieved less than 4% degradation in semi-transparent cells after 1000 h of MPP operation at 60 °C (Fig. 2d) [60].

Phase stabilization of perovskites using mixed cations can also be applied to inorganic $CsPbI_3$ materials. A range of solutions have been developed to stabilize α-$CsPbI_3$ at room temperature. Absorption studies of Snaith et al. showed that partial replacement of I by Br could increase the phase stability and prolong exposure to ambient atmosphere (hours or days depending upon the ambient humidity) (Fig. 2e). However, the composition change leads to an undesired increase in the bandgap [112]. Actually, $CsPbBr_3$ shows super stability against heat and humidity. The unencapsulated device demonstrates nearly unchanged performance under 80% relative humidity over 100 days and 85 °C over 30 days, but the record efficiency is only up to 11.08% due to the wide bandgap [113]. B-site substitution could also stabilize α-$CsPbI_3$. Zhang et al. demonstrated that the Bi-incorporated α-$CsPb_{0.96}Bi_{0.04}I_3$ maintains 68% of the initial PCE of 13.21% for 168 h under ambient conditions without encapsulation (Fig. 2f) [114]. Miyasaka et al. stabilized the α-$CsPbI_3$ at lower annealing temperature (85 °C) by incorporation of Eu^{3+} ($EuCl_3$) into $CsPbI_3$, which prevents the black to the yellow phase (δ-$CsPbI_3$) transformation in ambient air (room temperature) for a reasonably long time (>30 days) [115]. Hagfeldt et al. demonstrated that Eu is incorporated into the $CsPbI_2Br$ perovskite lattice on the atomic level by solid-state nuclear magnetic resonance (NMR) and high-angle annular dark-field scanning transmission electron microscopy (HAADF STEM). Hong et al. doped Eu^{2+} and In^{3+} into mixed halides $CsPbI_2Br$ to further enhance the stability. The fully air-processed devices exhibit stabilized efficiency of 17.05% for a small area (0.09 cm^2) and 15.04% for square-centimeter-scale cells, respectively. The unencapsulated PSCs maintain >95% and >75% of initial PCE over 400 h at 65 °C and 85 °C, respectively, revealing a robustness against thermal stress [116].

2D perovskite

2D perovskites are demonstrated to be promising candidates for optoelectronics due to their improved stability and additional functionalities compared to 3D perovskites [26,117,118]. The most studied Ruddlesden-Popper (RP) 2D perovskite has a structure of $(RNH_3)_2A_{n-1}B_nX_{3n+1}$, where R is an aromatic or aliphatic alkylammonium cation, A is Cs^+, $CH_3NH_3^+$ or $HC(NH_2)_2^+$, B is Pb^{2+} or Sn^{2+}, X is a halide ion, n defines the layer number of the perovskite sheets (Fig. 3a). As an artificial quantum-well with ideal two-dimensionality, 2D perovskites have been intensively studied for transport properties or exciton states in quantum-wells in the last decade before they were applied to optoelectronics [119,120].

In 2011, Chen et al. investigated the properties of 2D $(3\text{-}BrC_3H_6NH_3)_2CuBr_4$ to achieve a PCE of 0.021% with a p-i-n structured solar cell for the first time [121]. In 2014, Karunadasa et al. reported the layered perovskite $(PEA)_2(MA)_2Pb_3I_{10}$, which can act as an absorber in a solar cell with a PCE of 4.7%. They demonstrated that the powder X-ray diffraction (PXRD) pattern of the layered perovskite did not show additional peaks over 46 days under 52% humidity as well as the absorption spectra showed no significant changes, while the 3D counterpart showed a new phase after 4–5 days (Fig. 3b) [122]. 2D perovskites with low *n* values show enhanced stability compared to those with higher n values, although they exhibit worse performance due to the lower mobility and carrier lifetime [123]. The poor out-of-plane charge transport by the insulating organic cations between the conducting inorganic slabs is the main challenge for improving the efficiency. To address this issue, vertically oriented quasi-2D perovskites were developed later by the hot-casting deposition [124] or processing with additives [125,126]. Thus, highly efficient 2D perovskite solar cells with better stability can be achieved using this approach. In 2016, Mohite et al. fabricated vertically oriented $(BA)_2(MA)_3Pb_4I_{13}$ by hot-casting for a solar cell with a significantly enhanced PCE of 12.5%. Both unencapsulated and encapsulated devices showed much-enhanced stability under illumination or 65% humidity compared to the 3D perovskite devices (Fig. 3c). Under illumination, the PCE degraded to about 50% of its original value within the first 10 h in the 3D encapsulated device and then saturated at approximately 10% of its original value after 800 h. In contrast, the 2D encapsulated perovskite devices were extremely robust, with no degradation and negligible hysteresis over 2250 h of constant illumination. With humidity of 65%, the PCE of an encapsulated 3D perovskite device decreases to < 10% of its original value over 350 h. In contrast, the encapsulated 2D devices do not exhibit any degradation in the first 650 h and maintain at 85% over 2085 h [124]. Recently, Huang et al. achieved high-performance solar cells and LEDs by using 3-bromobenzylammonium iodide (3BBAI) based quasi-2D perovskite film. The unencapsulated devices sustain over 82% of their initial efficiency after 2400 h under relative humidity (RH) of ≈ 40% and show almost unchanged photovoltaic parameters after immersion into water for 60 s. On the other hand, the external quantum efficiency of electroluminescent devices (EQE_{EL}) decays to half of the initial value after ≈ 96 h of continuous operation at a given current density of 200 mA cm^{-2}, creating a new record for operation lifetime of perovskite LEDs, which is also even better than the best performing near-infrared organic LEDs [127].

Although 2D perovskites with $n = 1$ show better stability than that of 2D perovskites with higher n [123], there are only a few works on their optoelectronic applications mainly due to the poor out-of-plane mobility and large bandgap. Recently by designing the organic spacer cations, the photovoltaic performance of $n = 1$ 2D perovskite was much enhanced. Stupp et al. reported a series of $n = 1$ layered perovskites with the form $(aromatic\text{-}O\text{-}linker\text{-}NH_3)_2PbI_4$. By tuning the aromatic moiety and linker, the out-of-plane conductivity was enhanced, resulting in a champion PCE of 1.38%. The synthesized 2D perovskite can withstand immersion in water for several minutes without

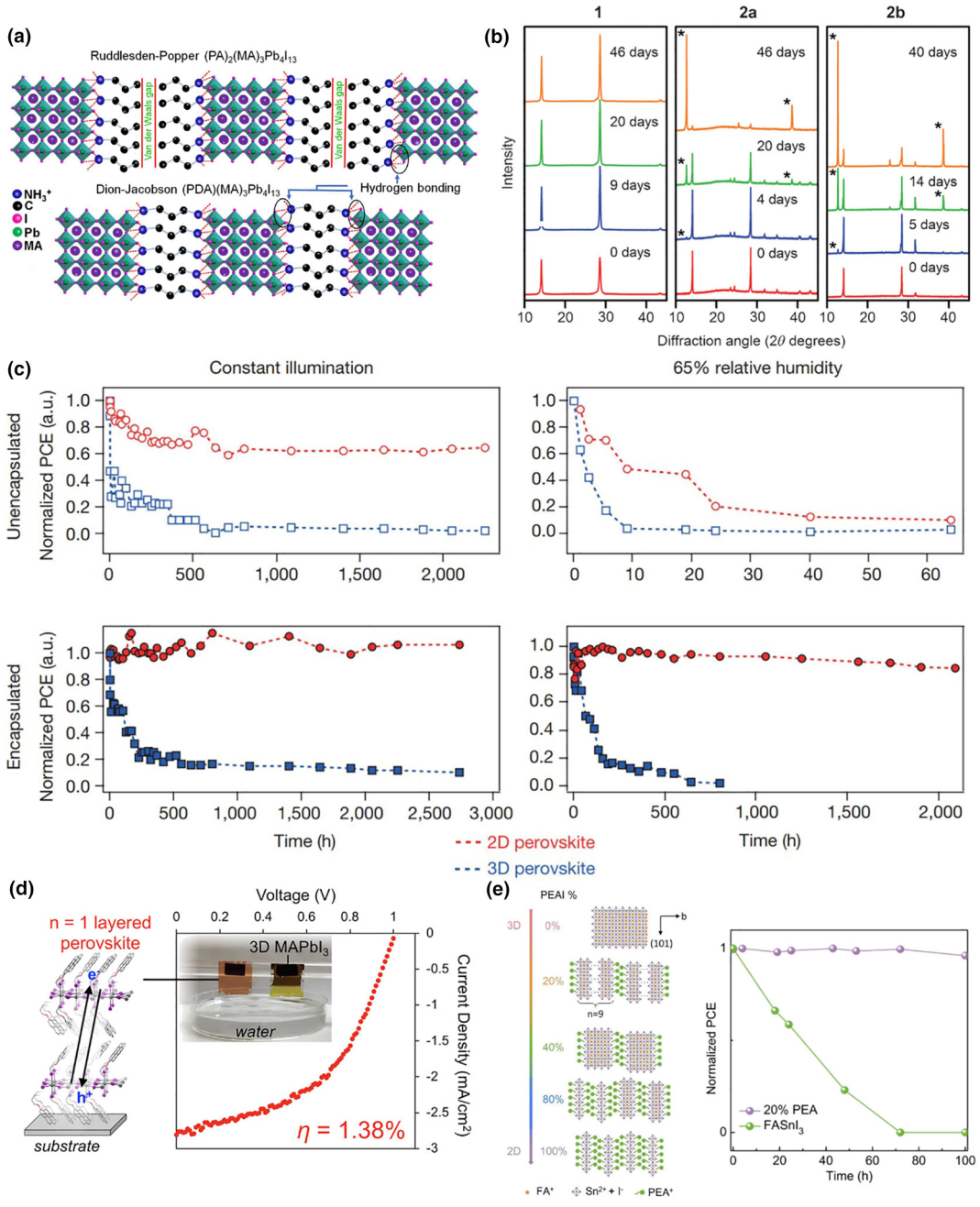

FIGURE 3

(a) Schematic illustration of RP and DJ phase 2D layered perovskites. Reprinted from [132], Copyright (2019), with permission from Elsevier. (b) PXRD patterns of films of $(PEA)_2(MA)_2Pb_3I_{10}$ (1), $MAPbI_3$ formed from PbI_2 (2a), and $MAPbI_3$ formed from $PbCl_2$ (2b), which were exposed to 52% relative humidity. Reproduced with permission of [122]. Copyright 2018 John Wiley & Sons, Inc. (c) Photostability tests under constant AM1.5G illumination and humidity stability for 2D $(BA)_2(MA)_3Pb_4I_{13}$ and 3D $MAPbI_3$ perovskite devices without and with encapsulation. Reprinted by permission from Springer Nature [124], Copyright (2016). (d) Schematic and *J–V* curve for the champion device based on (pyrene-O-propyl-NH_3)$_2PbI_4$ layered perovskite. The photograph (inset) shows the difference in the appearance of two substrates after dipped in water: $MAPbI_3$ turned yellow instantly revealing chemical degradation, whereas the n = 1 layered perovskite (pyrene-Opropyl-NH_3)$_2PbI_4$ retained its original color. Reprinted with permission from [128]. Copyright 2018 American Chemical Society. (e) Schematic structures of $FASnI_3$, $(PEA)_2SnI_4$ and mixed FA-PEA tin perovskites. Normalized PCE of the unencapsulated device based on $FASnI_3$ and 20% PEA-doped perovskite film stored in a glovebox for over 100 h. Reprinted with permission from [133]. Copyright 2017 American Chemical Society.

any decomposition to lead iodide (Fig. 3d) [128]. Nazeeruddin et al. synthesized 2D perovskites with symmetrical imidazolium-based cations such as benzimidazolium (Bn) and benzodiimidazolium (Bdi), which show relatively narrow band-gaps compared to traditional $-NH_3^+$ amino groups, at 1.81 eV and 1.79 eV for Bn_2SnI_4 and $BdiSnI_4$, respectively. Perovskite solar devices using Bn_2SnI_4 show promising efficiencies of up to 2.3%, but detailed stability studies have not been reported yet [129].

Tailoring the organic spacer cations could also enhance the stability of quasi-2D perovskites. Jen et al. demonstrated that MeO-PEAI and F-PEAI-based quasi-2D perovskites (n = 5) show

much better stability in air (RH ~40–50%) than PEAI-based quasi-2D perovskites. This is due to the steric effect and electron repulsion of MeO and F to the water lone pair electrons which could prevent water from penetrating into the perovskite structures [130]. Recently, Huang et al. designed a new bulky alkylammonium, 2-(methylthio)ethylamine hydrochloride (MTEACl). In addition to a weaker van der Waals interaction, the interaction between sulfur atoms in two MTEA molecules enables a $(MTEA)_2(MA)_4Pb_5I_{16}$ (n = 5) perovskite framework with enhanced charge transport and stabilization. The result is 2D RP PSCs with significantly improved efficiency and stability compared with those based on butylammonium iodide (BAI) which is only one atom different. PSCs with a power conversion efficiency as high as 18.1% (17.8% certified) are achieved, along with moisture tolerance for up to 1512 h (under 70% humidity conditions), thermal stability for 375 h (at 85 °C) and stability under continuous light stress (85% of the initial efficiency retained over 1000 h of operation at the MPP) [131].

Dion-Jacobson (DJ) phase 2D perovskites with the formula of $A'A_{n-1}B_nX_{3n+1}$, where A' represents a divalent organic cation, have the potential to stabilize the layered perovskite structure by eliminating of the van der Waals gap (Fig. 3a). Li et al. demonstrated that the DJ phase 2D perovskites exhibit greater material and device stabilities than the RP phase counterparts by comparing the 2D perovskites derived from the 1,3-propanediamine (PDA) and the propylamine (PA) cations, respectively [132]. Relative to the PSCs based on the RP phase 2D perovskite, the DJ phase analogs not only resulted in a higher PCE of 13.3%, but also exhibited a higher stability, retaining more than 95% of PCE, when subjected to very harsh testing conditions such as ambient air with 40%–70% RH for 4000 h, heating at 85 °C under 85% RH for 168 h, and continuous light soaking in a nitrogen-filled glove box for 3000 h.

Apart from the greater moisture resistance, the layered structure may also greatly enhance the air stability of Sn-based perovskite materials. Ning et al. demonstrated the improved oxidation resistance of low-dimensional Sn perovskite $(PEA)_2(FA)_{n-1}Sn_nI_{3n+1}$ using the same approach. When n = 9, the 2D PSC shows a PCE of 5.9% and retains 96% of its initial value for over 100 h, while the PCE of 3D $FASnI_3$ PSC decays by 77% within 48 h in a glove box without encapsulation (Fig. 3e) [133]. Further optimization of the film processing technique and addition of NH_4SCN into $PEA_{0.15}FA_{0.85}SnI_3$ resulted in a record PCE of 9.41%. The device sustains 90% of its initial PCE for nearly 600 h after storing in a nitrogen-filled glovebox [134].

Besides, reducing the dimension of perovskite could significantly suppress the undesirable phase transition of α-$CsPbI_3$. Chen et al. demonstrated reduced-dimensional α-$CsPbI_3$ perovskite photovoltaics with greatly improved performance longevity, and showed that quasi-2D perovskites with lower n values (n = 10) exhibit better phase stability than those with higher n values (n = 40, 60) [135].

2D/3D perovskite

Quasi-2D perovskites have shown significant improvement in stability but poorer performance compared to their 3D counterparts. 2D/3D mixed perovskite with high nominal n values (typically n > 10) may combine the advantages of 2D and 3D perovskites, achieving high performance and high stability simultaneously. Due to the passivation ability of 2D perovskites, 2D/3D perovskites could even achieve higher performance than their 3D counterparts.

Snaith et al. obtained a thin 2D perovskite film, where the butylammonium (BA) cation was orientated perpendicularly to the plane of the film embedded between 3D perovskite grains. The devices show improved PCE and much better stability compared to their 3D counterparts. Cells sustain 80% of their 'post-burn-in' efficiency after 1000 h and close to 4000 h when encapsulated. The devices are aged under xenon-lamp simulated full-spectrum AM1.5, 76 mW cm^{-2} equivalent irradiance in air with a humidity of ~45% without any ultraviolet filter, held at open-circuit during ageing, and tested at different time intervals under a separate AM1.5, 100 mW cm^{-2} solar simulator [136]. Yang et al. also demonstrated that 2D perovskite spontaneously forms at grain boundaries of 3D perovskite, protects the FA perovskite from moisture and suppress ion migration. Thereby a stabilized PCE of 20.64% (certified stabilized PCE of 19.77%) with significantly enhanced operational stability was achieved (Fig. 4a) [64].

Other than improving stability against moisture, as mentioned in the previous section, 2D/3D structures could also enhance the phase stabilities of perovskites as quasi-2D structure. Jen et al. revealed that introduction of PEAI into $FAPbI_3$ perovskite to form mixed cation $FA_xPEA_{1-x}PbI_3$ can effectively enhance both phase and ambient stability of $FAPbI_3$. The ambient stability of the $FA_xPEA_{1-x}PbI_3$ (FA/PEAI = 40, nominal n ≈80) based device is greatly improved, which retains over 90% of its initial PCE (17.71%) after being stored in air for 16 days under a relative humidity of 40 ± 5% without encapsulation. Contrarily, the PCE (14.05%) of pure $FAPbI_3$ based device decays to near zero after 16 days [63]. Zhao et al. stabilized the α-$CsPbI_3$ films by introducing a small amount of ethylenediamine cations (EDA^{2+}) to form a 2D/3D structure. The resulting α-$CsPbI_3$ structures are highly robust at room temperature for months and can retain their phase even after annealing at 100 °C for a week. The best solar cell based on the $CsPbI_3{\cdot}0.025EDAPbI_4$ perovskite showed good stability because it retained its ~10%-efficiency after storing in a dark, dry box for one month without any encapsulation [137]. Chen et al. also demonstrated that quasi-2D $PEA_2Cs_{n-1}Pb_nI_{3n+1}$ perovskites with lower n values (n = 10) exhibit better phase stability than those with higher n values (n = 40, 60) (Fig. 4b). After 40 days under ambient atmosphere without sealing, the devices kept 98%, 93%, 83%, 83% and 77% of the initial values for n = 10, 40, 60, 80 and 100 quasi-2D perovskites, respectively [135]. Meng et al. utilized phenyltrimethylammonium iodide (PTAI) to enhance the phase stability of $CsPbI_3$, it could also effectively suppress non-radiative recombination in the PSC devices. As a consequence, the champion PSC device based on $CsPbI_3$ exhibits a record efficiency of 21.0% with high stability [138]. Other than those strategies, Steele et al. recently found that substrate clamping and biaxial strain could render black-phase $CsPbI_3$ thin films stable at room temperature [57].

2D/3D structure could also suppress the phase separation of mixed-halide wide-bandgap perovskites, which is particularly detrimental to the performance of both LEDs and solar cells. Rand et al. achieved phase-stable mixed halide perovskites by

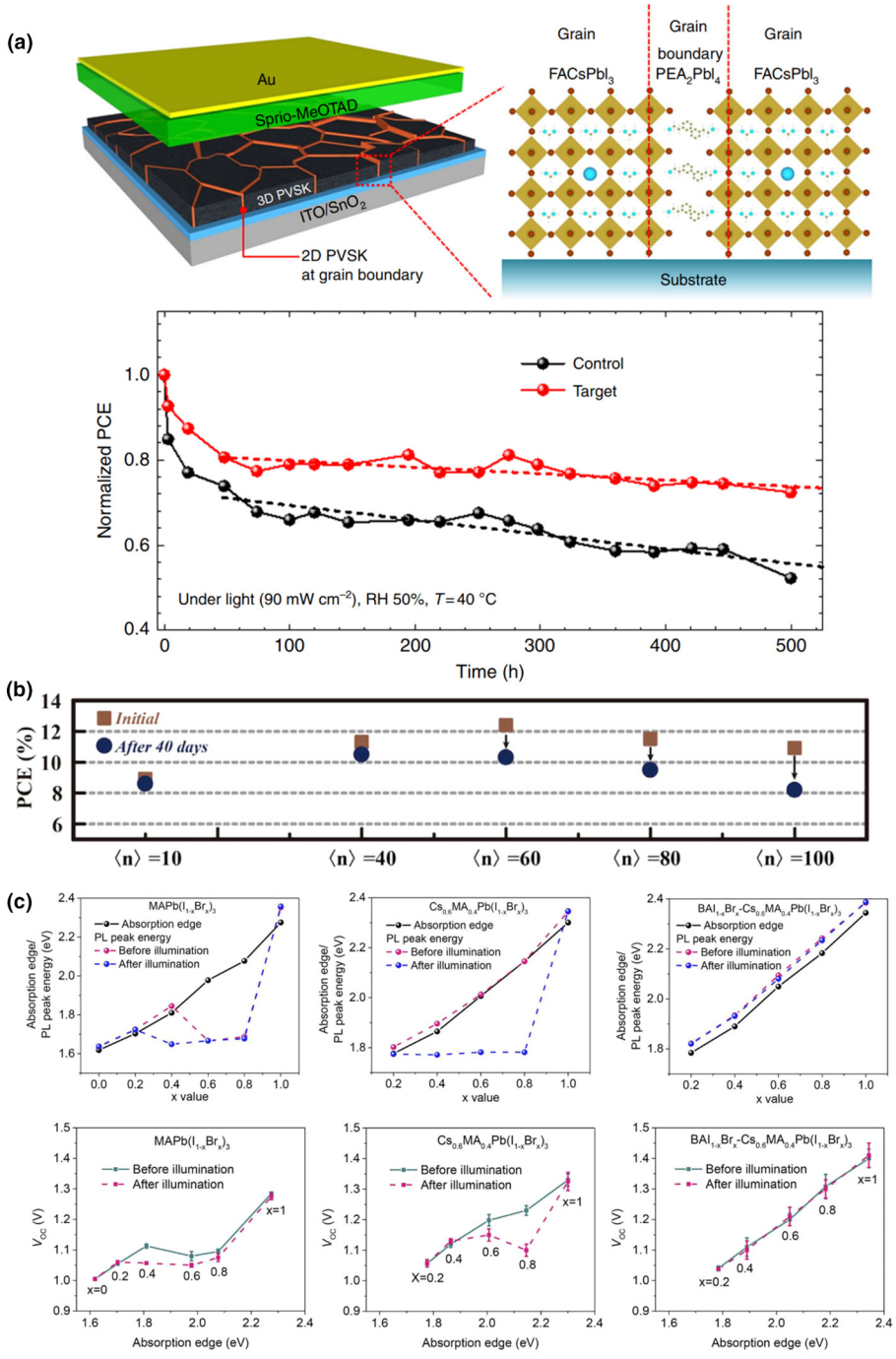

FIGURE 4

(a) Schematics of the device incorporating polycrystalline 3D perovskite film with 2D perovskite at grain boundaries and evolution of the PCEs measured from the encapsulated control and target devices exposed to continuous light (90 ± 5 mW cm^{-2}) under open-circuit condition. The stabilized PCEs were measured at each time. Initial stabilized PCEs for control and target devices were 14.5% and 17.5%, respectively. Reprinted by permission from Springer Nature [64], Copyright (2018). (b) Stability of quasi-2D $PEA_2Cs_{n-1}Pb_nI_{3n+1}$ perovskites (n = 10, 40, 60, 80, 100) perovskite-based devices under ambient atmosphere without sealing. Reprinted from [135], Copyright (2018), with permission from Elsevier. (c) Summary of the optical absorption edge, PL peak energy and V_{OC} versus the x values of the mixed-halide films before and after illumination. Reprinted with permission from [101]. Copyright 2017 American Chemical Society.

adding BAI, which could be used to fabricate high-efficiency LEDs with tunable emission wavelengths and solar cells with tunable V_{OC} (Fig. 4c) [101]. Jen et al. also demonstrated that PEA incorporation can reduce the extent of phase segregation of large bandgap perovskite $MAPb(I_{0.6}Br_{0.4})_3$ under light, thus improving V_{OC} and light stability [102].

2D/3D perovskite were successfully prepared by depositing ammonium halides or amines to form thin 2D perovskite layers on top of a 3D perovskite film. Nazeeruddin et al. attained the surface of a 2D perovskite layer by spin coating a PEAI solution on an optimized lead excess pristine $Cs_{0.1}FA_{0.74}MA_{0.13}PbI_{2.48}Br_{0.3}$ perovskite film. The devices based on 2D/3D perovskite films

show enhanced performance and impressive improved stability at 50 °C in air, retaining 90% of the initial PCE after 800 h under continuous illumination in inert gas condition and 85% at humid environment with encapsulation [139]. *n*-Butylamine (BA) was used to obtain a 2D/3D stacking structure by Huang et al., with thin layers of $(BA)_2PbI_4$ on top of 3D perovskite. After reacting with BA, the corresponding devices show enhanced performance (17.28% to 19.29%) and much improved thermal stability in comparison to the 3D counterpart or BAI-modified counterpart when subjected to the heat stress test. The control device degraded to 69.8% of its initial efficiency after continuous heating for 100 h, while the BA and BAI modified devices still maintained 96.5 and 88.2% of their initial efficiencies [140].

Phase stable perovskite quantum dot

Stabilization of the unstable α-phase perovskites such as $CsPbI_3$ and $FAPbI_3$ can also be archived by reducing all three dimensions in the form of perovskite QDs [141,142]. These perovskite QDs, with sizes generally around 4–12 nm, have made remarkable advancements in the field of QD based LEDs, with external quantum efficiencies (EQEs) around 12%, 22% and 15% in the blue, green, and red parts of the visible spectrum, respectively [143], but also as sensitizers in solar cells [144,145], with certified efficiencies almost reaching 17% [146]. On the one hand, the large surface areas of these QDs raises significant challenges in term of chemical stability, for instance, towards moisture degradations. Although challenging, perovskite QDs allow for the generally unstable α-phase perovskites, in the form of $CsPbI_3$ and $FAPbI_3$, to be significantly more stable than their bulk counterparts. This nanoscale stabilization can be ascribed to the high surface area of the QDs, which in combination with careful tuning of their surface ligands can lead to surface strain, which results in pressure-induced α-phase stabilization [82]. Luther et al. demonstrated that the careful surface treatment of $CsPbI_3$ QDs can result in QD films being stable for months in ambient air when treated with suitable ligands. They also developed a method for perovskite QD film assembly to remove the long and insulating organic capping ligands which significantly hinder the carrier transport between neighboring QDs, allowing for efficient dot-to-dot electronic transport while retaining the phase stability of the individual QDs. Finally, an efficiency of 10.77% is achieved for the first perovskite QD-based photovoltaic cell, which were tested completely in ambient conditions after 15 days (relative humidity ~15 to 25%) (Fig. 5a) [82]. Further ligand chemistry as well the chemical interface engineering has resulted in $CsPbI_3$ QD based solar cells achieving a PCE surpassing 14% [31]. The initially assigned purely cubic α-phase of $CsPbI_3$ QDs was later corrected to be a lower symmetry orthorhombic γ-phase [147]. Similar to the $CsPbI_3$ QDs, pure $FAPbI_3$ QDs also seem to gain from the ligand-induced surface strain, allowing them to be significantly more stable compared to bulk $FAPbI_3$ [148]. Xue et al. for instance, demonstrated that $FAPbI_3$ QD films show significantly better ambient and operational stability compared to bulk films, where QDs remain stable over months. Pure $FAPbI_3$ QDs based solar cells show similar PCEs as those based on $CsPbI_3$ QDs, with the current record certified efficiency at 13.2% (Fig. 5b) [149]. Br and Cl-based QD formulations could also stabilize $FAPbBr_3$ and $FAPbCl_3$, although their tolerance factors are outside of the stable perovskite range [150,151].

Perovskite QDs also seem to have an additional benefit compared to bulk perovskites, as they have much higher miscibility with mixed cations with suppressed phase segregation due to the small crystalline domain of the individual QDs. This was demonstrated by a full range of $Cs_xFA_{1-x}PbI_3$ QDs with x = 0–1, resulting in room temperature stable QDs for any given x composition (Fig. 5c) [152]. The combined suppressed phase segregation and ligand-induced phase stabilization were recently utilized by Hao et al. to demonstrate a $FA_{0.5}Cs_{0.5}PbI_3$ QDs solar cell with a certified efficiency of 16.6%, which is currently the highest for any type of QD based solar cell (Fig. 5d) [146]. Further device optimization and the use of $CsPbI_3$ QDs deposited on top of $Cs_{0.25}FA_{0.75}PbI_3$ QDs creating a charge separating heterostructure has resulted in the current non-certified QD solar cell conversion efficiency surpassing 17% [153]. The high cation miscibility of perovskite QDs is also visible for B site alloying, allowing for a wide variety of divalent metal cations and further improving the $CsPbI_3$ stability by increasing their goldsmith tolerance factors [154]. These cations for instance include Mn^{2+}, Zn^{2+} and Sr^{2+} (Fig. 5e) [155,156], where the latter has been used to further stabilize $CsPbI_3$ QDs for use in red light LEDs with efficiencies up to 15% [145].

Overall, perovskites QDs pose a unique solution tackling the phase instabilities observed with $CsPbI_3$, $FAPbI_3$ and mixed perovskites. Since perovskite QDs have also achieved high photoluminescence quantum yield, they are very attractive for other optoelectronic devices like LCDs and LEDs, as further discussed in Sections “Liquid crystal display” and “Light-emitting diode” respectively.

Devices

Advances in technology depend on integrating new materials, the emerging materials such as 2D materials [32,157], conducting polymers [158] have quickly become the hottest directions of research in the world and widely utilized into the fields of photonics, optoelectronics, catalysis, biomedicine, and energy applications. In the following sections, the strategies of how to enhance the stabilities in terms of different kinds of perovskite devices will be discussed.

Solar cell

Thin-film solar cells based on perovskites have so far reached record PCE up to 25.7% in certified measurements [15,159]. Separation and extraction of photogenerated carriers are based on selective carrier contacts; thus the perovskite absorber is sandwiched between wide-bandgap ETL and HTL with suitable work functions. High PCEs can be achieved by careful engineering of the interfaces, to minimize non-radiative recombination and resistance losses, and reduction of structural defects in the perovskite bulk as well as passivation of grain boundaries. Application of perovskite in photovoltaic modules, their acceptance and market uptake require extended reliability testing and device stability testing standards adapted to this technology.

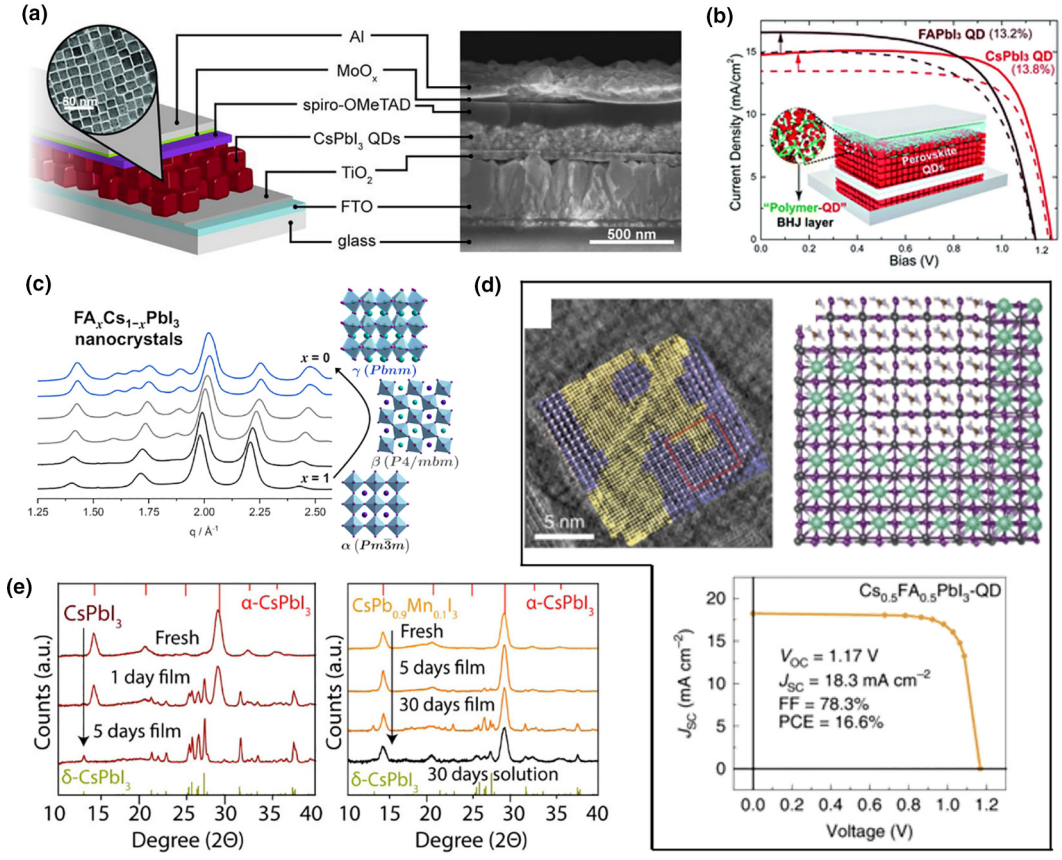

FIGURE 5

Overview of perovskite quantum dot-based phase stabilisation and solar cells. (a) First demonstrated solar cell using $CsPbI_3$ QDs, demonstrating an efficiency exceeding 10% which is stable up to month. From [82]. Reprinted with permission from AAAS. (b) Most recent pure $FAPbI_3$ and $CsPbI_3$ QD dot solar cells exceeding 13%. Reproduced from Ref. [149] with permission from the Royal Society of Chemistry. (c) Integrated 1D grazing incidence wide-angle X-ray scattering (GIWAXS) patterns and crystallographic phases of $FA_xCs_{1-x}PbI_3$. Reprinted with permission from [152]. Copyright 2020 American Chemical Society. (d) Phase segregation stabilization within a single $Cs_{0.5}FA_{0.5}PbI_3$ QD, showing limited segregation due to small QD crystalline domain. Using this concept, a record perovskite QD cell efficiency of 16.6 % was obtained. Reprinted by permission from Springer Nature [146], Copyright (2020). (e) Example of phase stabilization using B site cation alloying. XRD diffraction analysis proves phase stability of $CsPb_xMn_{X-1}I_3$ QDs for over one month. Reprinted with permission from [155]. Copyright 2017 American Chemical Society.

Charge-transporting layers

Ideal transport layers should efficiently extract photogenerated charge carriers from the perovskites but also protect the perovskite layers from exposure to moisture or air. Currently, the most widely used ETL in n-i-p structured devices is TiO_2. However, a critical instability in mesoporous TiO_2-sensitized solar cells was reported, arising from light-induced desorption of surface-adsorbed oxygen (Fig. 6a) [29]. Therefore many suitable and reliable metal oxides have been explored as alternative ETLs, such as ZnO [160], Zn_2SO_4 [161], CdSe [162], CdS [163] and SnO_2 [164]. CdS and CdSe, which have also been successfully applied in Cu(In,Ga)Se solar cells, are toxic, and ZnO can react easily with perovskites during thermal annealing (>100 °C) [165]. Today, SnO_2 appears to be the most promising candidate and can be processed at low temperatures [164,166]. Perovskite cells with SnO_2 ETLs achieve very high PCEs and avoid the drawbacks of UV-light instability that occurs when using TiO_2 [167,168]. Modification of metal oxide ETLs by self-assembly monolayers could also efficiently enhance the device performance and stability. For example, Jen et al. utilized a dual-functional interfacial material, 5-amino-2,4,6-triiodoisophthalic acid (ATPA), to interact with both $CsPbI_3$ perovskite and TiO_2 to achieve better energy tuning and surface passivation. As a result, a higher PCE with enhanced photostability are achieved [169].

The widely used and most efficient hole transport material (HTM), spiro-OMeTAD, for n-i-p structured devices, faces severe stability issues mainly due to the low glass transition temperature (T_g) and doping. Spiro-OMeTAD shows a low T_g of ~120 °C and decreases to ~50 °C when dopants are added. Therefore, annealing at high temperatures leads to the deformation of spiro-OMeTAD film arising from crystallization. Consequently, solar cells which employ additive-doped spiro-OMeTAD as HTL exhibit poor stability [170]. Seo et al. found that the device featuring an HTM with higher T_g showed better thermal stability than the device with spiro-OMeTAD, maintaining almost ~95% of its initial performance for more than 500 h after thermal annealing at 60 °C [171]. Dopants such as bis(trifluoromethylsulfonyl)imide lithium salt (Li-TFSI) and 4-*tert*-butyl pyridine (TBP) are necessary to increase the mobility of the spiro-OMeAD, but they are hygroscopic and can capture the atmospheric moisture, and thus accelerate the moisture-induced degradation of the perovskite layer [172]. Therefore many novel dopant-free organic HTM are

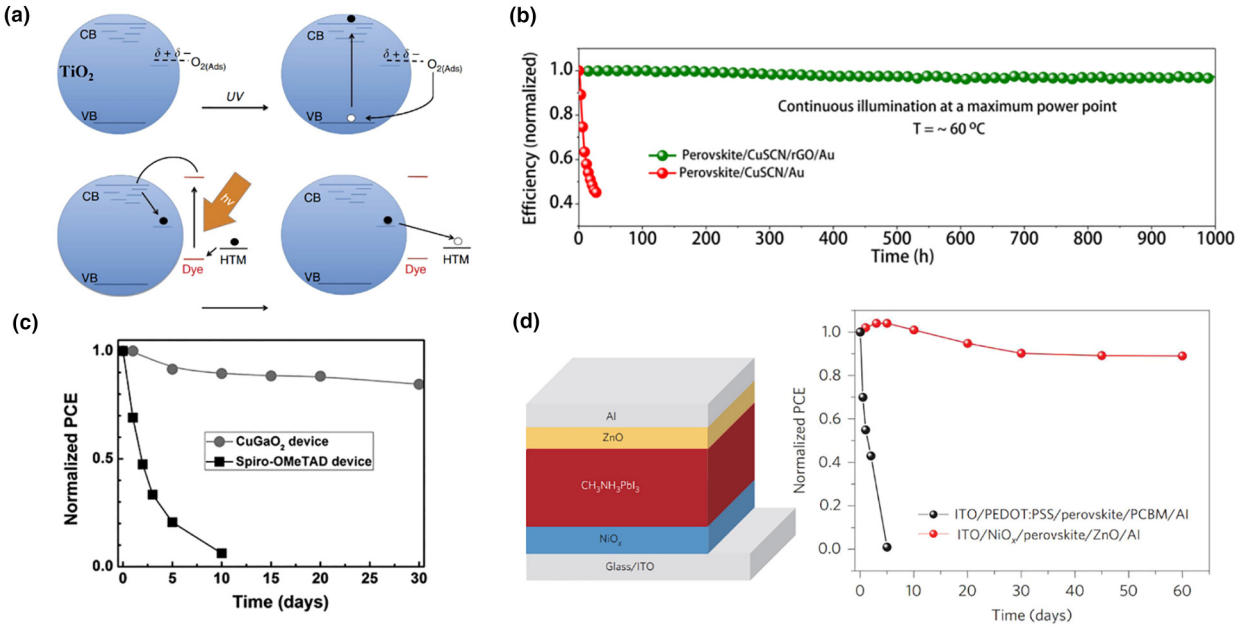

FIGURE 6

(a) Mechanism for UV-induced degradation in TiO_2 based perovskite solar cells. Reprinted by permission from Springer Nature [29], Copyright (2013). (b) Normalized efficiency of un-encapsulated CuSCN based PSCs with and without a thin layer of rGO spacer layer between CuSCN and gold layers. Operation stability was examined at a maximum-power point under continuous full-sun illumination at 60 °C in nitrogen atmosphere. From [179]. Reprinted with permission from AAAS. (c) Comparison of device stability of an optimized $CuGaO_2$-based and a spiro-OMeTAD based-device measured under ambient environment (30%–55% humidity, T = 25 °C). Reproduced with permission of [180]. Copyright 2017 John Wiley & Sons, Inc. (d) Device structure and PCE stability of PSCs with different ETL and HTL in an ambient environment without encapsulation. Reprinted by permission from Springer Nature [28], Copyright (2016).

developed to improve device stability while maintaining high performance [172–174]. For example, Liu et al. synthesized a solution-processable 2D polymer HTM, 2DP-TDB, with dominant face-on packing orientation, good charge transport properties, efficient perovskite surface passivation capability and hydrophobicity. Thus, PSCs based on dopant-free 2DP-TDB HTM show a champion efficiency as high as 22.17%. The unencapsulated devices could sustain over 95% of their initial efficiency after stored in the ambient atmosphere (RH = 30 ± 5%) for 1000 h, whereas only 64% of original efficiency left for the devices with typically doped spiro-OMeTAD [175]. Besides, modification of the perovskite/HTL or HTL/electrode interface may improve the stability. It was shown, that adding 1-adamantylammonium iodide into the HTM, enabled retention of the PCE value within a few percent after 500 h under continuous light illumination of unencapsulated devices under an inert atmosphere [176]. Noh et al. incorporated gallium(III) acetylacetonate ($Ga(acac)_3$) into HTMs without hygroscopic dopants and it could spontaneously interact with the surface of the perovskite layer, yielding a reduction of the interfacial recombination loss for various organic HTMs. The $Ga(acac)_3$-devices show superior moisture stability for 2000 h under 85% relative humidity at room temperature without any encapsulation, maintaining a complete initial performance of 21.8%. An enhanced PCE of 24.6% is achieved with aligned P3HT as HTM. This is the highest efficiency reported for conventional PSC based on dopant-free HTM [177]. Deposition of a thin layer of rubrene can cover the pinholes of the spiro-OMeAD layer, which improves device stability after 100 h under continuous light illumination, retaining 97% of its initial performance compared with 65% of the reference device [178]. On the other hand, inorganic HTLs such as CuSCN [179] and $CuGaO_2$ [180] are developed, which can efficiently replace the less stable spiro-OMeTAD. Grätzel et al. demonstrated that PSCs using CuSCN HTL and a conductive reduced graphene oxide spacer layer between CuSCN and gold allowed the reduced the degradation of >20%-efficient devices to <5% after aging at a maximum power point for 1000 h at 60 °C. Importantly, under both continuous 1-sun illumination and thermal stress, CuSCN based devices surpassed the stability of spiro-OMeTAD based PSCs (Fig. 6b) [179]. Jen et al. fabricated an efficient PSC employing solution processed $CuGaO_2$ as HTL. It exhibits an impressive PCE of 18.51%, higher than the device using spiro-OMeTAD, and shows significantly improved long-term stability (Fig. 6c) [180].

For p-i-n devices, poly(3,4-ethylenedioxythiophene) polystyrene sulfonate (PEDOT:PSS) is widely used even though it is not an ideal HTM due to inefficient electron-blocking capability and poor chemical stability stemming from its hygroscopic nature. CuSCN [181], NiO_x [182,183], NiMaLiO [184] and copper (II) phthalocyanine (CuPC) [185] have been demonstrated to be promising alternative HTM. By combing p-type NiO_x and n-type ZnO nanoparticles as HTL and ETL respectively, Yang et al. achieved highly efficient and highly stable PSCs. After 60 days of storage in air at room temperature, the fabricated all-metal-oxide based device retained about 90% of the original efficiency (Fig. 6d) [28].

Defects engineering

Structural defects which are mainly located at grain boundaries (GBs), surfaces and interfaces provide primary channels for ion migration and act as initiation sites for moisture, oxygen, and light-induced degradation [186–189]. Water penetration also occurs preferentially by the diffusion of water molecules through defect-rich perovskite facets, mainly found at surface and grain boundaries [70,190]. Depending on the growth conditions and growth methods, dominant defects can vary and so do the diffusion species as well as diffusion mechanisms, leading to different degradation behaviors [191]. Meng et al. demonstrated that electric field-induced interface defects have a stronger impact on stability than bulk defects. Introducing a fullerene derivative stress-buffer-layer is an effective route to decrease interface defect states, due to suppressed lattice strain, and improves stability [192]. Thus, surface modification, reducing grain boundaries and passivation can improve the stability of the perovskite materials and devices as well as improve the device performance by reducing non-radiative recombination.

Huang et al. demonstrated that quaternary ammonium halides can effectively passivate ionic defects in several different types of hybrid perovskites which boosts the PCE to a certified value of 20.6 ± 0.5% and also significantly enhances the stability of films in ambient conditions (Fig. 7a) [193]. Zhou et al. employed fluoride to simultaneously passivate both anion and cation vacancies, by taking advantage of its extremely high electronegativity. They exhibited a PCE of 21.5% (certified 21.3%) based on $Cs_{0.05}FA_{0.54}MA_{0.41}PbI_{2.94}Br_{0.06}$ perovskite treated with sodium fluoride. The device retained 90% of its original PCE after 1000 h of operation at the MPP [194]. Stranks et al. stabilized the photoinduced ion migration across a wide range of mixed halide perovskite bandgaps by decorating the surfaces and grain boundaries with a passivating potassium halide layer. The passivation also reduced the non-radiative recombination and increased charge transport, thus high performance was achieved (Fig. 7b) [195]. Yang et al. used natural products theophylline, caffeine, and theobromine to passivate antisite Pb (lead) defects. The encapsulated device with theophylline treatment maintained >90% of its initial efficiency (21.3%) in 500 h compared to degradation by more than 80% for the reference device, when tracked at an RH of 30–40% and a temperature of 40 °C [196]. Ionic liquids are another kind of efficient additives to improve the device efficiency and stability. Snaith et al. observed a degradation in performance of only around 5% for the encapsulated device under continuous simulated full-spectrum sunlight for more than 1800 h at 70–75 °C with 1-butyl-3-methylimidazolium tetrafluoroborate ($BMIMBF_4$) as additive. The enhanced performance and stability are due to the reduced surface defect density and suppressed ion migration [197]. Later, they found that $BMIMBF_4$ could also supress the phase segregation which is mainly caused by ion migration in wide bandgap perovskite $Cs_{0.17}FA_{0.83}Pb(I_{0.77}Br_{0.23})_3$. Thus, the device with enhanced open-circuit voltage and efficiency is achieved. Furthermore, the unencapsulated and encapsulated cells retain 80 and 95% of their peak and post-burn-in efficiencies for 1010 and 1200 h at 60° and 85 °C, respectively [198].

Increasing grain size, thus reducing the number of grain boundaries, is another efficient way to reduce the trap state density. Zhao et al. utilized a MABr-selective Ostwald ripening process to increase the grain sizes of $MAPbI_3$ film, which improved both cell efficiency and device stability [199]. Grätzel et al. added MACl as a crystallization aid to the precursor to realize high-quality, large-grain triple-cation perovskite films. The devices showed enhanced operational stability, and retained 96%, 90% and 85% of their initial PCE values after 500 h under continuous light illumination at 20, 50, and 65 °C, respectively [200].

Especially hydrophobic molecules, which may also chemically passivate the perovskite surface defects, can efficiently improve the perovskite stability [187,201]. Zhu et al. introduced guanidinium thiocyanate (GuaSCN) to improve the structural and optoelectronic properties of low bandgap $(FASnI_3)_{0.6}(MAPbI_3)_{0.4}$ perovskite thin films. Gua^+ and SCN^- ions tend to segregate at GBs to form 2D structures, which appear to passivate defect states, suppress the formation of excessive Sn vacancies, and enhance the stability of low-bandgap perovskite films [202]. Huang et al. converted the surfaces of lead halide perovskite to water-insoluble lead (II) oxysalt through reaction with sulfate or phosphate ions which effectively stabilized the perovskite surface and bulk material. This boosted the PCE to 21.1% by reducing the defect density. Encapsulated devices stabilized by the lead oxysalt layers maintain 96.8% of their initial efficiency after operation at MPP under illumination for 1200 h at 65 °C (Fig. 7c) [187]. Han et al. stabilized the $FA_xMA_{1-x}Pb_{1+y}I_3$ perovskite layer by forming strong Pb–Cl and Pb–O bonds between perovskite film with a Pb-rich surface and a chlorinated graphene oxide layer. The PSCs show PCEs approaching 21% with a cell area of 1.02 cm^2 exhibiting excellent operational stability, maintaining 90% of its initial PCE value after operation at the MPP under 60 °C for 1000 h [203].

Quasi-2D perovskites were demonstrated to be more stable than 3D perovskites against humidity or under illumination [124], yet they still show limited stability under sustained photoexcitation and electrical injection, and this remains a roadblock to their application in LEDs. Sargent et al. developed an edge-stabilization strategy wherein phosphine oxides passivate unsaturated lead sites during the quasi-2D perovskite crystallization. The passivated quasi-2D perovskite shows significantly enhanced PL stability (Fig. 7d). Furthermore, the green LED device showed a longest operational lifetime of 3.5 h at high luminance (4000 cd m^{-2}), which is 21 times higher compared to the best prior report (at the initial luminance of 3800 cd m^{-2}, with T50 = 10 min) [204]. This strategy should also enhance operation stability of quasi-2D PSCs.

Device stability testing standards

International standards were established by the International Electrotechnical Commission (IEC), which defines standard testing procedures to evaluate the performance and stability of industrial photovoltaic modules [205]. The IEC 61215:2016 Damp Heat, Thermal Cycling, and Humidity Freeze tests (Table 1) are among the standard accelerated tests specified for commercial modules. The modules must survive these tests with less than 5% relative loss in efficiency [206]. Since a large number of research groups with different backgrounds are working on emerging next generation solar module technologies such as organic, dye-sensitized and perovskite solar cells,

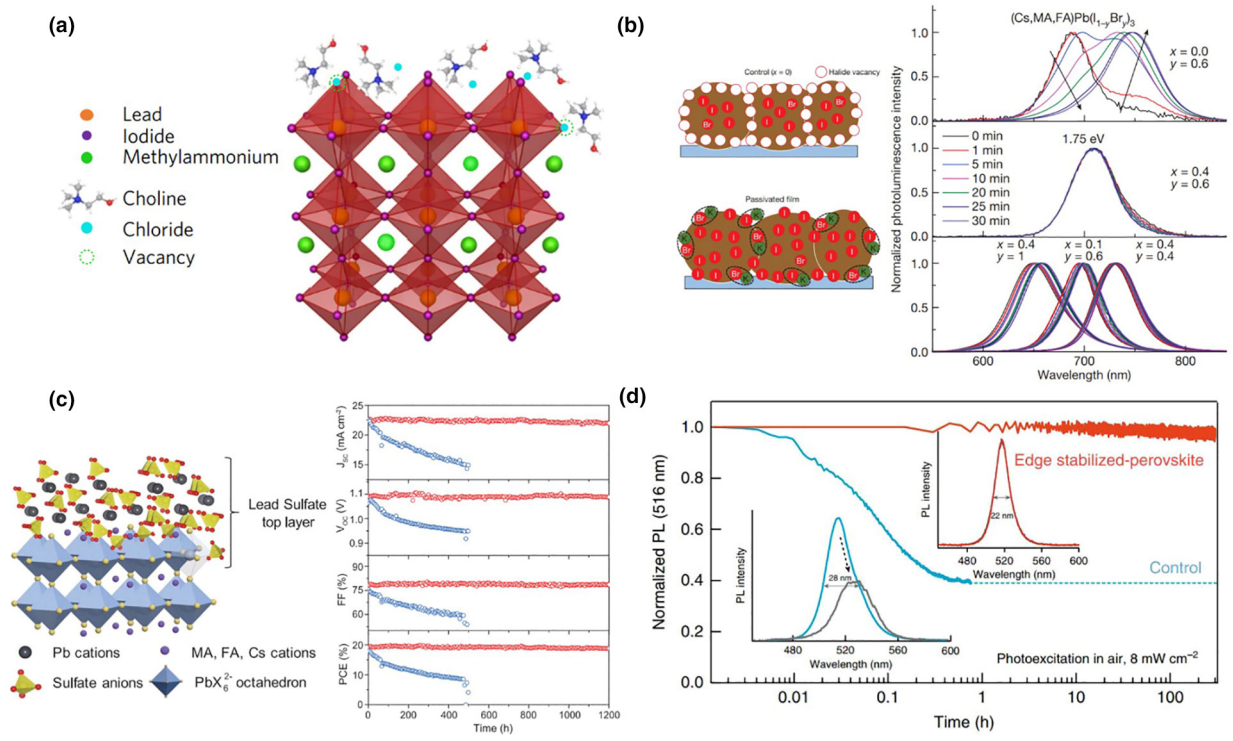

FIGURE 7

(a) Schematic illustration of quaternary ammonium halides (QAHs) assembled on the defect sites. The red and blue symbols represent the N atom and O atom of the choline chloride molecule, respectively. Reprinted by permission from Springer Nature [193], Copyright (2017). (b) PL spectra of (Cs,FA,MA)Pb($I_{1-y}Br_y$)$_3$ without passivation (x = 0) and with potassium passivation (x = 0.1, 0.4) (x = [K]/([A] + [K]), illuminated continuously under the same conditions. Reprinted by permission from Springer Nature [195], Copyright (2018). (c) Schematic illustration of protection of perovskites through in-situ formation of a lead sulfate top layer on the perovskite surface and stability test of encapsulated solar cell devices based on control (blue) and sulfate-treated (red) CsFAMA perovskite active layers without UV filter in air (relative humidity ~60 ± 10%). From [187]. Reprinted with permission from AAAS. (d) PL intensity stability of quasi-2D perovskites under continuous excitation under a 374 nm laser diode. The inset shows PL spectra of the untreated control and edge-stabilized sample before (in red and blue, respectively) and after (in grey) measurement. Reprinted by permission from Springer Nature [204], Copyright (2020).

TABLE 1

Specifications of the three IEC 61215:2016 tests.

Test	Damp test	Thermal Cycling test	Humidity freeze test
Condition	85 °C	− 40 °C (15 min dwell) to 85 °C (15 min dwell), Ramp rate of 100 °C/hour	50 rounds of Thermal Cycling as prerequisite, followed by − 40 °C (30 min dwell) to 85 °C, 85% RH (20 h dwell). Ramp rate of 100 °C/hour for 0 °C ↔ 85 °C; Ramp rate of 200 °C/hour for 0 °C ↔ − 40 °C
Requirement	1000 h	200 cycles	10 cycles

there is an increasing demand for standard methods to accurately measure the efficiency in a lab environment [207]. Several articles have discussed in detail general issues and challenges related to the correct characterization and have provided recommendations [207–209]. Nevertheless, there are still no binding standards for stability testing methods. This lack of standards leads to the lack of consistency in the assessment and reporting procedures, which hinders data comparison [210]. Recently a large group of 59 scientists in the field of PSCs have presented consensus on procedures for studying the stability of PSCs [211].

Liquid crystal display

Lead halide perovskite QDs, as discussed in Section "Phase stable perovskite quantum dot", have attracted significant attention as color conversion layers (CCLs) for LCDs (Fig. 8a, b) [212]. The benefit of using perovskite QDs in LCDs originates in part from their high color turnability and narrow emission linewidth, allowing for a higher color purity compared to OLEDs and conventional phosphors, thus allowing for the full coverage of the color gamut (up to 90% of Rec.2020 standard), as well as from their high PLQY, which allows for a high brightness (near unity). Furthermore, the defect tolerance of perovskite QDs eliminates the need for careful surface passivation techniques like core shell QDs or removing defects with hydrofluoric acid (HF) [213], significantly reduces the production cost of perovskite QDs for display applications compared to other QDs like CdSe and InP [214,215]. To this extend, green emitting $CsPbBr_3$ QDs (515–525 nm), which emit closely to the ideal green emission around 532 nm, are predicted to reach consumer LCDs within the next

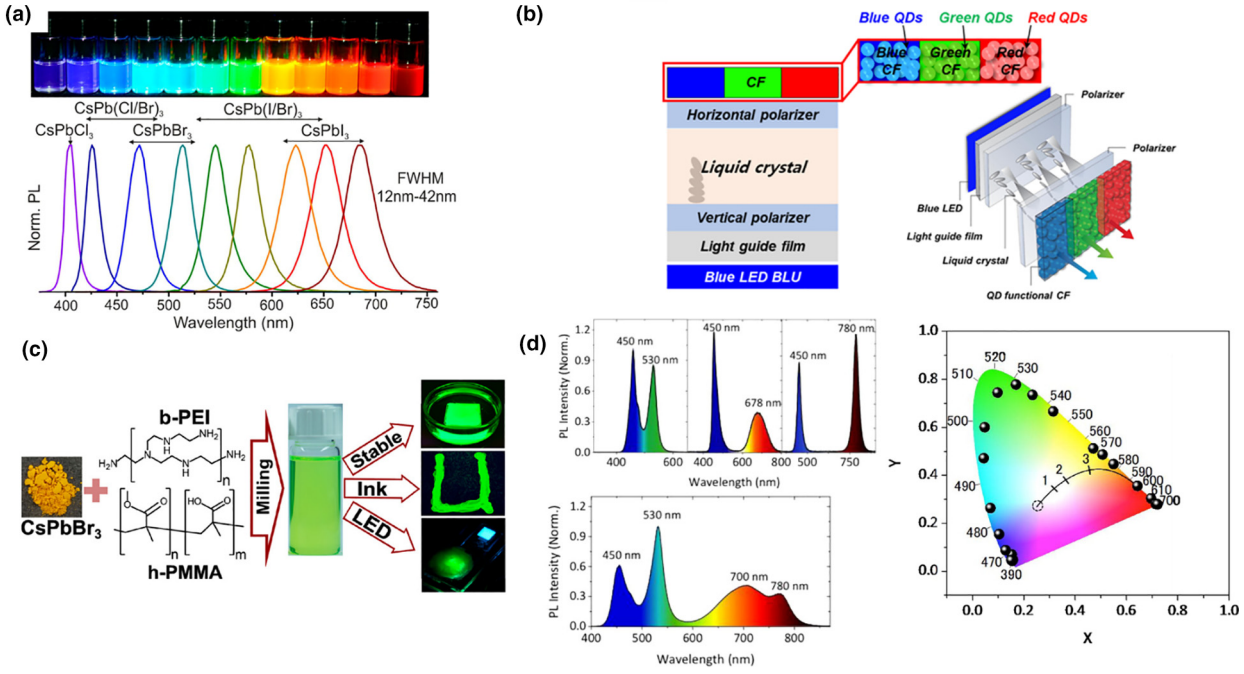

FIGURE 8

(a) $CsPbX_3$ nanocrystals (X = Cl, Br, I) exhibit size- and composition-tunable bandgap energies covering the entire visible spectral region with narrow and bright emission. Reprinted with permission from [142]. Copyright 2015 American Chemical Society. (b) Schematic structures of LCDs with quantum-dot functional color filter (QD-functional CF) and blue LED back-light unit (BLU). Magnified image in (b) shows the structure of QD-functional CF and the right image in (b) shows the 3D schematic structure of QD-functional CF LCD. Reprinted by permission from Springer Nature [23], Copyright (2018). (c) Scheme of the perovskite nanocrystals preparation applying ball milling of the solid precursors in the presence of h-PMMA and b-PEI as stabilizing polymers. Reprinted with permission from [221]. Copyright 2019 American Chemical Society. (d) Stacking various crystal/polymer films of selective emission wavelengths on a commercial blue LED (450 nm emission) (left-up). Stacking the films can achieve white light with a desired color rendering index. The right figure shows the chromaticity color coordinates (CIE) plotted from the corresponding perovskite crystal emissions marked as 1, 2, 3, respectively. Reprinted with permission from [225]. Copyright 2015 American Chemical Society.

few years [216]. On the other hand, $FAPbBr_3$ NCs, which exhibit a slightly smaller bandgap, can cover the ideal 532 emission [217]. These FA-based QDs though are significantly less chemically and thermodynamically stable compared to their $CsPbBr_3$ counter parts, which makes the production of LCDs displays more challenging. Further optimization of such systems using $FAPbBr_3$ with careful surface as well as device passivation will most likely allow to exchange the green emission from $CsPbBr_3$ with $FAPbBr_3$ and thus reach the ideal green in LCD (and LED) technologies. The coverage of blue (467 nm) as well as red (630 nm) emitting parts of LCDs with perovskite QDs still remains challenging, as the emission the $CsPbCl_3$ (around 410 nm) and $CsPbI_3$ NCs (680 nm) does not reach the ideal emission. Furthermore, using halide alloying to reach the required values results in halide migration and segregation after long exposure, thus limiting their use. Likewise, using quantum confinement to reach for instance the blue emission using small $CsPbBr_3$ QDs results in significantly broadening of the PLQY, and thus lowering the color purity [143]. Using 2D confinement, such as $CsPbBr_3$ nanoplatelets, which show significantly narrower PL at the same wavelength of $CsPbBr_3$ QDs, as well as 2D perovskites can reach these ideal values and thus might stable, bright and narrow blue emission for LCDs [218].

The typical reliability tests for displays demand layers with a robust tolerance (<15% drop in intensity) to temperatures as high as 90 °C, moisture as high as 95% and flux up to 400 mW cm^{-2}. Unfortunately, the chemical degradation of perovskites gets accentuated at these conditions and hence the most significant challenge that needs to be solved for this application is once again their stability. Common strategies used to improve the stability of perovskite LCDs include (i) compositional engineering (doping of A and B-sites); (ii) surface engineering (ligands and trap state passivation); and (iii) matrix encapsulation with polymers and oxides [219].

For the structural stability of perovskites, the ionic radius plays a key role. Utilizing all-inorganic $CsPbBr_3$ systems with higher thermal and environmental stability have demonstrated widespread success [45]. Zhu et al. synthesized red-emitting $CsPbBr_{1.2}I_{1.8}$ perovskite QDs *via* a Br-I alloying route in a poly (methyl methacrylate) (PMMA)/chloroform solution with enhanced moisture tolerance. Yttrium aluminium garnet (YAG)-coated white light-emitting diodes (WLEDs) were demonstrated with a color rendering index (CRI) of 92, CCT of 4222 K, and luminous efficacy of 78.4 lm W^{-1}, superior to bare YAG-based WLED (CRI of 74 and CCT of 6713 K) [220]. Utilizing partially hydrolyzed poly(methyl methacrylate) (h-PMMA) and highly branched poly(ethylenimine) (b-PEI) as double ligands, Gaponik et al. demonstrated stable perovskite nanocrystal CCLs with excellent stability against water, heat, and ultraviolet light irradiation (Fig. 8c). The hydrophobic polymer of h-PMMA imparted excellent film-forming properties and water stability, while the b-PEI passivated the surface of the nanocrystals and

promoted growth of a $CsPbBr_3/CsPb_2Br_5$ core–shell-like structure resulting in enhanced PLQY and stability. 80% of the PL of the perovskite nanocrystals–polymer composite was retained when placed under water for 40 days. After six heating/cooling cycles (25 °C/120 °C) or being treated under a 2 W UV light lamp (dominant wavelength at 365 nm) for as long as 120 h, the PL intensity of h-PMMA/b-PEI-capped perovskite nanocrystals film retained 70% and about 60% of its initial value respectively. In comparison, the PL intensity of OLA/OA-capped perovskite nanocrystals encapsulated in PMMA dropped to about 10% and 15% of its initial value respectively under the same conditions [221]. In general, polymer encapsulants such as poly (methyl methacrylate) (PMMA), ethyl cellulose, polystyrene (PS) and mesoporous silica have been widely utilized with varied success [222–224]. By tailoring the composition of methyl and octylammonium cations, Snaith et al. reported the formation of meso- to nanoscale 3D $MA(OA)PbX_3$ crystals with an enhanced photoluminescence efficiency. By blending perovskite crystals of different emission wavelengths in a PS host over a blue GaN LED chip, white light emission with a CRI of 86 and CCT of 5229 K was demonstrated (Fig. 8d) [225]. Lin et al. demonstrated efficient white light emission with chromaticity coordinates of $x = 0.31$, $y = 0.30$, by packing all-inorganic green $CsPbBr_3$ and red $CsPb(Br_{0.4}I_{0.6})_3$ perovskites into cross-linked PS beads using a swelling-shrinking strategy [226]. This resulted in good robustness against water, acid-aqueous and alkali-aqueous solutions while maintaining high luminescence. Wang et al. exploited super-hydrophobic frameworks to stabilize $CsPbBr_3$ QDs with narrow-band emission, high PLQY, and excellent water stability of 6 months. A WLED device was successfully fabricated based on green-emitting $CsPbBr_3$ QDs by embedding the QDs into the super-hydrophobic porous organic polymer frameworks. In combination with red-emitting KSF phosphors, and a blue LED chip, high luminous efficiency of 50 lm W^{-1} and a wide color gamut (127% of NTSC, 95% of Rec. 2020) was demonstrated [227].

2D perovskite structures with strong van der Waals interactions, developed by introducing long-chain amines such as oleylamine into the perovskite structure, portray enhanced stability than their 3D counterparts, and play vital roles in this regard. Density functional theory (DFT) calculations have revealed higher desorption energy for PEAI from the perovskite structure, 0.36 eV higher than that for MAI, pointing to 1000 times slower decomposition than $MAPbI_3$ films in ambient conditions [122]. Facile incorporation of organic cations into the perovskite lattice has triggered considerable research interest recently in creating hybrid 2D–3D perovskite films and core–shell structures with good device performance and long device lifetimes. However, this is still at its nascent stage and entails further systematic investigations [228–230].

Light-emitting diode

Perovskites have emerged as promising semiconductors for light-emitting applications because of their high color purity and excellent photoluminescence quantum efficiencies [231–235]. The performance of LEDs using perovskite as the emissive layer (PLEDs) has witnessed an unprecedented rise in recent years, reaching EQE values as high as 28.1% [236–239].

PLEDs were first developed using 3D perovskites, with a focus on homogenous film morphology and small grain sizes [233]. Subsequently, mixed-dimensional perovskites and assemblies of colloidal perovskite nanocrystals have attracted attention for high-efficiency PLEDs because of the enhanced confinement of charge carriers as well as effective radiative recombination [142,240–243]. Irrespective of the type of perovskite emitter adopted, it is necessary to efficiently eliminate non-radiative recombination routes to achieve high-performance. Utilization of quasi-core–shell structures [244], perovskite–polymer heterostructures [245] and hydrogen bonding manipulation [236] have enabled EQEs of PLEDs over 20%, approaching those of organic LEDs (OLEDs).

Similar to photovoltaics, several strategies are necessary to ensure high performance and operational stability. At the material design level, this includes enhancing the radiative bimolecular recombination rate [233], exploiting radiative excitonic recombination (Fig. 9a) [246], suppressing trap-assisted non-radiative recombination (Fig. 9b) [247] and controlling non-radiative Auger recombination [248]. At the device level, the interlayer properties can in turn affect the crystallinity, morphology, defect properties and energy level structures of the perovskite layers [249]. Chemical interactions at the perovskite–interlayer interfaces are more intricate, and their effects on PLED performance warrant additional exploration.

Among the challenges that currently impede further development of PLEDs such as mediocre performance (especially for red and blue emission) and toxicity of Pb-containing active materials, the poor operational stability warrants maximum attention. The operational lifetime of PLEDs (10^2 h range) [245,250,251] still lags behind those of commercial organic LEDs, which exceeds 10,000 h under constant electrical stress. It is worth noting that the operational stability limitations of PLEDs are due to the low maturity of the technology. Hence, further studies on the perovskite degradation, i.e., thermal, moisture and photostability, and its mechanisms are required to move towards practical implementations of PLEDs. The factors responsible for the poor stability of PLEDs mainly include ion migration, thermal instability and interfacial instability, similar to photovoltaics.

Although much attention has been paid to the pathways of extrinsic degradation of perovskites, e.g., the influence of moisture and oxygen, intrinsic degradation pathways induced during the device operation such as ion redistribution and related atomistic and morphological effects such as the role of grain boundaries, etc. have not been explored systematically yet. The electric field applied to perovskite devices may trigger diverse electrochemical degradation pathways, which are significant to LEDs, but these are still poorly investigated. Bias-assisted microscopy and spectroscopy techniques have revealed numerous possibilities of electrochemical degradation mechanisms existing within the device architecture.

Troshin et al. observed both reversible oxidation of I^- to I_2 (which remains trapped in the film as polyiodides) and an irreversible reduction of organic methylammonium cations under applied electric bias utilizing atomic force microscopy, photoluminescence mapping and time-of-flight secondary ion mass spectrometry (ToF-SIMS) (Fig. 9c) [252]. Similar observation on field-induced migration of MA^+ cation to the cathode was

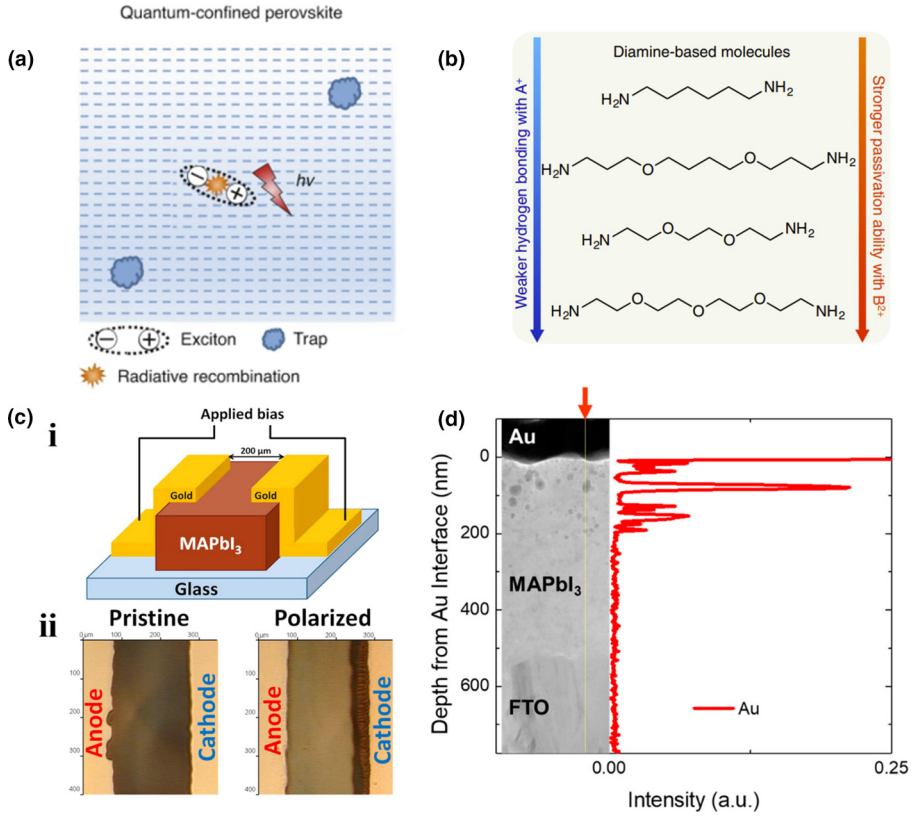

FIGURE 9

(a) A schematic illustration of charge-carrier recombination in quantum-confined perovskites. (b) An illustration demonstrating the modulation of passivation effects by rational molecular design. Reprinted by permission from Springer Nature [263], Copyright (2020). (c) General layout of the lateral two-electrode device (i). Optical microphotograph of the device channel before (left) and after (right) applying 1 V μm^{-1} bias for 340 h (ii). Reprinted with permission from [252]. Copyright 2020 American Chemical Society. (d) STEM image and EDX line profile of Au in an FTO/$MAPbI_3$/Au device biased at 0.9 V for 6 h. Reprinted with permission from [85]. Copyright 2020 American Chemical Society.

revealed *via* photothermal infrared (PTIR) microscopy by Huang et al., thus evidencing the often ignored contribution of organic cations to the ionic conductivity of halide perovskites [253].

The effect of electrode materials and transport layers on the electrochemical stability of perovskite films is also not well studied, which is an essential issue for LEDs. For example, migration of oxygen ions from the TiO_x electron transport layer to the perovskite film was confirmed *via* electron energy loss spectroscopy (EELS) measurements by Shin et al. [254]. This activated a significant structural transformation of single-crystalline $MAPbI_3$ grains to their amorphous state with the appearance of PbI_2 and could be partially restored under reverse bias. Very recently, Rand et al. showed clear evidence of electrochemical oxidation of gold (the "noblest of metals") at the $MAPbI_3$/Au and HTM-buffered interfaces with threshold voltages of 0.8 and 1.2 V, respectively *via* ToF-SIMS, scanning transmission electron microscopy (STEM), and energy-dispersive X-ray spectroscopy (EDX) measurements (Fig. 9d) [85]. This points to continuous electrochemical reactions occurring within the device during its operation. Such reactions may result in an evolution of intermediate products within the device, changing its characteristics reversibly or irreversibly. Gao et al. found that generation of halide vacancies at perovskite/hole transport layer interface during operation is one of the dominant degradation pathways in PLEDs. The accumulated halides within the hole transport layer undergo back diffusion toward the surface of the perovskite layer during resting, repairing the vacancies and thus resulting in electroluminescence recovery. By passivating the key interface, PLED with a high external quantum efficiency of 22.8% and obviously improved operational stability is achieved [16]. Furthermore, Janaky et al. reported expulsion of iodine from the lattice of mixed halide perovskite ($CH_3NH_3PbBr_{1.5}I_{1.5}$) films upon hole trapping. This results in the reformation of $CH_3NH_3PbBr_3$ domains that act as charge carrier recombination centers, providing insight into the photoinduced phase segregation of perovskite thin-film devices [255].

Reduction of Pb^{2+} to Pb^0 is likely to be another major long-term problem for lead halide perovskite devices. Using *in situ* XRD measurements and scanning electron microscopy (SEM), Rand et al. observed moisture-accelerated interfacial redox reactions of Pb^{2+} to Pb^0 in perovskite devices equipped with various metals such as Ag, Al, Yb and Cr as a function of their standard electrochemical potentials [256]. Choi et al. reported that Br vacancies at non-passivated surfaces could trigger reduction of Pb^{2+} to Pb^0 by trapping electrons generated from exciton dissociation [257]. Further evidence of redox reactions was confirmed by Ginger et al. via multimodal microscopy combining *in situ* photoluminescence and scanning Kelvin probe microscopy in a lateral electrode geometry. By comparing trap formation with both charges injecting and blocking contacts, the reduction of

Pb^{2+} to Pb^0 in $MAPbI_3$ was observed only in the presence of injected electrons, suggesting the possibility of redox processes with injected electronic charge [258].

Proposed strategies to enhance the device stability include the use of bulky organic ligands and interface engineering. Xiao et al. suggested the incorporation of bulky organic ligands in the perovskite structure to effectively stabilize the surface, preventing ion migration [259]. Gao et al. utilized the dicarboxylic acids in the precursor to efficiently eliminate reactive organic ingredients in perovskite emissive layers through an in situ amidation process, which is catalyzed by the alkaline zinc oxide substrate. The formed stable amides prohibit detrimental reactions between the perovskites and the charge injection layer underneath, stabilizing the perovskites and the interfacial contacts and ensuring the excellent operational stability of the resulting PLEDs. Efficient PLEDs with a peak external quantum efficiency of 18.6% and a long half-life time of 682 h at 20 mA cm^{-2} is achieved [260]. Further improvements are proposed by reducing the Joule heating through interface engineering [261] or employing amino-acids additives as passivation layers [250].

Whereas industrial device stability testing standards for photovoltaic modules have been readily adapted for perovskite solar cells, stability test for perovskite LEDs are not as well defined. This has made directly comparing both the performance as well as stability of perovskite LEDs difficult. Therefore, similar to perovskite photovoltaics, we suggest the development of a universal stability protocol for PLEDs [211]. To this extend T50 or T95 values should always be reported, which correspond to the time it takes for an LED to drop to 50% or 95% of its initial output [262]. For such measurements, no well-defined conditions are established, and therefore it is important to report as main parameters as possible (such as luminesce, voltage, LED size etc.). Establishing and pre-defining, such operation and devices requirements to a fixed set of parameters (as with solar cells) would greatly help to compare perovskite LEDs in a trusted and consistent manner [262,263]. Consistent lifetime and color stability tests under similar operational and atmospheric conditions would be of great relevance to assess the numerous degradation pathways in various PLED systems, which would boost the technology evolution.

Ionizing radiation detectors, transistors and memristors

Ionizing radiation detecors are no less susceptible to the stability issues of halide perovskites in comparison to photovoltaics and LEDs. While material characteristics such as large light absorption coefficient, incorporation of heavy elements such as Cs^+, Pb^{2+}, Ag^+, Bi^{3+}, Sn^{2+}, tuneable bandgap, high mobility, long carrier recombination lifetimes, large bulk resistivity and defect tolerance promise strong stopping power, low dark currents and noise, and good radiation hardness; self-doping, polarization and operational instability adversely affects the performance of these materials [264–266]. The polarization effect, a consequence of ion migration, results in a continuous shift of the dark current and degrades the energy spectral resolution of the detector. Hence, all the above-discussed strategies to suppress ion migration find relevance here as well. Noteworthy contributions in this regard include alloying, partial substitution of FA^+ and I^- with Cs^+ and Br^- [267], dopant compensation [268] and engineering of the electrical contacts [269].

Transistors are the basic building blocks of all electronic circuits, used to amplify or switch electrical signals and power. Despite the remarkable advances in photovoltaics and LEDs, realization of perovskite field-effect transistors (FETs) remains challenging [270]. This can be mainly attributed to their poor gate modulation abilities due to partial screening of the applied gate field induced by ion migration. Admittance, dielectric loss and Raman spectroscopy measurements have also identified charged point defects located at grain boundaries, polarization fluctuation of the A-site cations, and lack of long-range crystalline order as detrimental factors [271]. While cryogenic operation (wherein the ions are frozen), utilizing single crystals with low defect densities and source-drain contact engineering with suitable interlayers have helped to mitigate the issue to some extent, perovskite FETs still suffer from non-ideal transistor characteristics with large hysteresis, bias stress instability and threshold voltage shifts upon continuous operation. The strategies to combat migration of ions via grain boundaries and surface defects in the perovskite film include increasing the grain size via excess use of acetates in the precursor chemistry [271], adopting molecular cross-linkers via hydrogen bond interactions between perovskite halogens and dangling bonds present at grain boundaries (Fig. 10a) [272], incorporating strain-relieving cations like Cs and Rb which act as passivation/crystallization modifying agents (Fig. 10b) [273], treating perovskite films with positive azeotrope solvents [273], and utilizing an auxiliary ferroelectric gate of poly(vinylidenefluoride-co-trifluoroethylene) [P(VDF-TrFE)], to electrostatically fixate the mobile ions (Fig. 10c) [274].

With the rise of artificial intelligence and machine learning, and experimental discovery of memristors (memory + resistor) [275], investigation of halide perovskites as memristive materials has lately attracted significant attention [89,90,276]. In contrast to other device technologies presented in this review such as photodetectors and LEDs, memristors could reap benefit from the migration of ions [277]. Mechanistically, halide perovskites support a rich variety of switching physics including electrochemical metallization reactions with reactive electrodes [278,279] and valence change mechanisms via halide ion migration [280,281], making them viable memristive materials for information storage and brain-inspired computer architectures. However, yield, stability and CMOS process incompatibility concerns continue to impede realization of crossbar arrays for large-scale implementations. This research direction is in its infancy and it remains to be seen whether insights derived from other device technologies can aid accelerated development of this new application for halide perovskites.

Sensors

The ionic perovskite crystals undergo reversible changes in structures/compositions under certain controlled conditions via phase transitions, hydration/dehydration, gas adsorption/desorption, and ion intercalation/decalation, suggesting their great potential for sensing applications [282], thus the perovskites have been reported as probes for sensing of gases [283–285], humidity [286,287], temperature [288], metal ions [289,290], water in solvents [291], and explosive species [292]. These studies

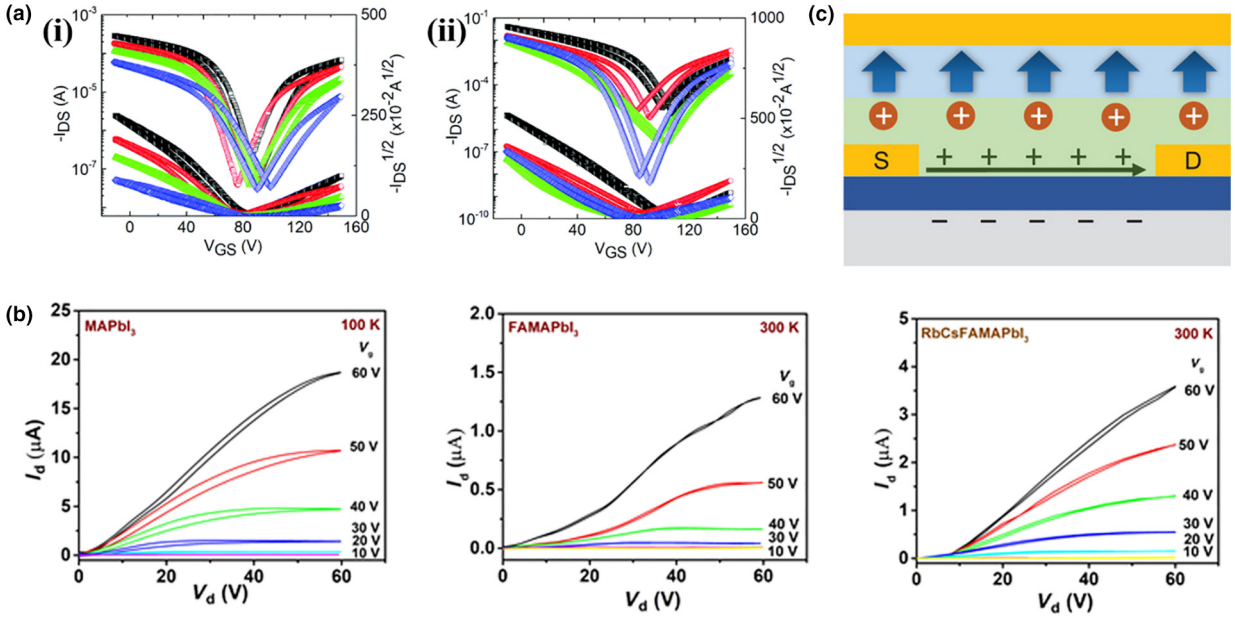

FIGURE 10

(a) Electron transfer characteristics of (i) unmodified and (ii) DPP modified-CsMAFA FETs at VDS = 100 V for electron operation measured at room temperature. Reproduced from Ref. [272] with permission from the Royal Society of Chemistry. (b) Output characteristics measured on the FETs based on $MAPbI_3$, $FAMAPbI_3$ and $RbCsFAMAPbI_3$ with L = 100 μm, W = 1 mm. From [273]. Reprinted with permission from AAAS. (c) Device operation with the negative polarization of the auxiliary ferroelectric gate at low gate voltages. Mobile cations are accumulated at the interface with the ferroelectric and holes are accumulated at the interface with the insulator to make a charge-transporting channel. Reproduced with permission of [274]. Copyright 2021 John Wiley & Sons, Inc.

indicate the potential of using perovskite sensors for practical uses with enhanced long-term stability by the strategies discussed above.

Summary and perspective

Since the first application as absorbers in solar cells, perovskites have been tested and employed into different kinds of devices, such as PSCs, LCDs, LEDs, ionizing radiation detectors, transistors, memristors and sensors due to their excellent optoelectronic properties. While rapid performance improvement has paved the way towards the commercialization of perovskite based devices, the long-term stability has become the main concern due to the intrinsically soft ionic crystal structures of perovskites. In this review, the instabilities, including thermal, phase, and environmental instability of the perovskite materials, are discussed as well as strategies to overcome them. Thoroughly investigating the entire material family for desired properties has the potential to further boost the performance and lifetime of perovskite devices. Reducing the dimensionality can stabilize perovskite materials and designing novel organic spacer cations could enable highly efficient and highly stable perovskite materials. Transport layers are crucial for device performance and stability, which should be carefully investigated. Ion redistribution is the bottleneck for LEDs, direct X-ray detectors. On the other hand, testing standards for different devices are urgently needed for data comparison in the assessment and reporting procedures.

Nowadays the most efficient optoelectronics are always using Pb-based halide perovskites. The high perceived toxicity of Pb has caused some concerns which may slow down or even hinder the pace of commercialization of Pb-based perovskite optoelectronics. Given the fact of the optoelectronic performance of the alternative lead-free perovskites are much worse, techniques of encapsulation and cyclization are encouraged to be developed to reduce the environmental impact for Pb-based perovskite devices. On the other hand, high performance and highly stable lead-free perovskites should also be encouraged to be developed.

Finally, currently most research on perovskite optoelectronics mainly concentrates on small lab-scale devices with an area of ~0.1 cm^2, increasing the device area decreases the device performance, thus upscaling perovskite optoelectronics while keeping efficient performance and stability is urgently needed.

Declaration of Competing Interest

The authors declare that they have no known competing financial interests or personal relationships that could have appeared to influence the work reported in this paper.

Acknowledgement

R.A.J. acknowledges the suport from the ETH Zurich Postdoctoral Fellowship scheme. M.S. thanks the German Research Foundation (DFG) for funding (SPP2196, 431314977/GRK 2642). M.S. and M.M.B. thanks the Helmholtz Young Investigator Group FRONTRUNNER. M.S. acknowledges funding by ProperPhotoMile. Project ProperPhotoMile is supported under the umbrella of SOLAR-ERA.NET Cofund 2 by The Spanish Ministry of Science and Education and the AEI under the project PCI2020-112185 and CDTI project number IDI-20210171; the Federal Ministry for Economic Affairs and Energy on the basis of a decision by the German Bundestag project number FKZ 03EE1070B and FKZ 03EE1070A and the Israel Ministry of Energy with pro-

ject number 220-11-031. SOLAR-ERA.NET is supported by the European Commission within the EU Framework Programme for Research and Innovation HORIZON 2020 (Cofund ERA-NET Action, No. 786483).

References

[1] D.P. McMeekin et al., Science 351 (2016) 151–155.
[2] F. Hao et al., J. Am. Chem. Soc. 136 (2014) 8094–8099.
[3] G.E. Eperon et al., Energy Environ. Sci. 7 (2014) 982–988.
[4] Q. Tai, K.-C. Tang, F. Yan, Energy Environ. Sci. 12 (2019) 2375–2405.
[5] A. Kojima et al., J. Am. Chem. Soc. 131 (2009) 6050–6051.
[6] D. Shi et al., Science 347 (2015) 519–522.
[7] S.D. Stranks et al., Science 342 (2013) 341–344.
[8] G. Xing et al., Science 342 (2013) 344–347.
[9] A. Miyata et al., Nat. Phys. 11 (2015) 582–587.
[10] G. Rainò et al., ACS Nano 10 (2016) 2485–2490.
[11] K.-H. Wang et al., Angew. Chem. Int. Ed. 55 (2016) 8328–8332.
[12] Z. Li et al., Nat. Rev. Mater. 3 (2018) 18017.
[13] Y. Dong et al., Small 15 (2019) 1902237.
[14] A.K. Jena, A. Kulkarni, T. Miyasaka, Chem. Rev. 119 (2019) 3036–3103.
[15] https://www.nrel.gov/pv/cell-efficiency.html.
[16] P. Teng et al., Matter 4 (2021) 3710–3724.
[17] Q. Zhang et al., Nano Lett. 21 (2021) 1903–1914.
[18] G. Li et al., Adv. Opt. Mater. 8 (2020) 1902012.
[19] C. Li et al., Nanoscale 12 (2020) 2201–2227.
[20] K. Chen et al., Nanoscale 11 (2019) 16852–16859.
[21] Y. Wang et al., Nanoscale 11 (2019) 2637–2643.
[22] L. Wu et al., Adv. Opt. Mater. 6 (2018) 1800400.
[23] Y.-H. Ko et al., Sci. Rep. 8 (2018) 12881.
[24] J.-P. Correa-Baena et al., Science 358 (2017) 739–744.
[25] M. Saliba et al., Energy Environ. Sci. 9 (2016) 1989–1997.
[26] J.L. Yan et al., J. Mater. Chem. A 6 (2018) 11063–11077.
[27] K. Chen et al., Coordin. Chem. Rev. 418 (2020) 213333.
[28] J. You et al., Nat. Nanotechnol. 11 (2016) 75–81.
[29] T. Leijtens et al., Nat. Commun. 4 (2013) 2885.
[30] D. Liu et al., Sol. RRL 2 (2018) 1800240.
[31] K. Chen et al., J. Am. Chem. Soc. 142 (2020) 3775–3783.
[32] Z. Xie et al., Chem. Rev. 122 (2022) 1127–1207.
[33] V. Poulek, A. Khudysh, M. Libra, Sol. Energy 120 (2015) 113–116.
[34] M. Benghanem, A.A. Al-Mashraqi, K.O. Daffallah, Renew. Energy 89 (2016) 51–59.
[35] G. Divitini et al., Nat. Energy 1 (2016) 15012.
[36] T. Baikie et al., J. Mater. Chem. A 1 (2013) 5628–5641.
[37] B. Conings et al., Adv. Energy Mater. 5 (2015) 1500477.
[38] E.J. Juarez-Perez et al., J. Mater. Chem. A 6 (2018) 9604–9612.
[39] R.K. Misra et al., J. Phys. Chem. Lett. 6 (2015) 326–330.
[40] A. Aziz et al., Chem. Mater. (2019).
[41] A. Binek et al., J. Phys. Chem. Lett. 6 (2015) 1249–1253.
[42] E.J. Juarez-Perez, L.K. Ono, Y. Qi, J. Mater. Chem. A 7 (2019) 16912–16919.
[43] N.J. Jeon et al., Nature 517 (2015) 476–480.
[44] L. Shi et al., Science (2020) eaba2412.
[45] M. Kulbak et al., J. Phys. Chem. Lett. 7 (2016) 167–172.
[46] A.F. Akbulatov et al., J. Phys. Chem. Lett. 8 (2017) 1211–1218.
[47] G.E. Eperon et al., J. Mater. Chem. A 3 (2015) 19688–19695.
[48] A.M.A. Leguy et al., Nanoscale 8 (2016) 6317–6327.
[49] J.-W. Lee et al., Adv. Energy Mater. 5 (2015) 1501310.
[50] W. Xiang, W. Tress, Adv. Mater. 31 (2019) 1902851.
[51] C. Wu et al., Adv. Sci. 5 (2018) 1700759.
[52] H.W. Lei, D. Hardy, F. Gao, Adv. Funct. Mater. 31 (2021) 2105898.
[53] B. Wang et al., J. Am. Chem. Soc. 143 (2021) 2207–2211.
[54] V.M. Goldschmidt, Naturwissenschaften 14 (1926) 477–485.
[55] Q.A. Akkerman, L. Manna, ACS Energy Lett. 5 (2020) 604–610.
[56] Z. Li et al., Chem. Mater. 28 (2016) 284–292.
[57] J.A. Steele et al., Science 365 (2019) 679–684.
[58] Z. Lin et al., Matter 4 (2021) 2392–2402.
[59] M. Saliba et al., Science 354 (2016) 206–209.
[60] J. Xu et al., Science 367 (2020) 1097–1104.
[61] J. Jeong et al., Nature 592 (2021) 381–385.
[62] H. Lu et al., Science 370 (2020) eabb8985.
[63] N. Li et al., Adv. Energy Mater. 7 (2017) 1601307.
[64] J.-W. Lee et al., Nat. Commun. 9 (2018) 3021.
[65] M. Saliba, Adv. Energy Mater. 9 (2019) 1803754.
[66] C.J. Bartel et al., Sci. Adv. 5 (2019) eaav0693.
[67] Y. Chen et al., Nature 577 (2020) 209–215.
[68] A. Waleed et al., Nano Lett. 17 (2017) 4951–4957.
[69] J.M. Frost et al., Nano Lett. 14 (2014) 2584–2590.
[70] A.M.A. Leguy et al., Chem. Mater. 27 (2015) 3397–3407.
[71] T.-B. Song et al., J. Am. Chem. Soc. 139 (2017) 836–842.
[72] F. Gu et al., C. ackwRRL 2 (2018) 1800136.
[73] D. Ricciarelli et al., ACS Energy Lett. 5 (2020) 2787–2795.
[74] S.J. Lee et al., J. Am. Chem. Soc. (2016).
[75] J. Cao et al., J. Mater. Chem. A (2019).
[76] X. Xu et al., Nano Energy 34 (2017) 392–398.
[77] K. Xiao et al., Nat. Energy 5 (2020) 870–880.
[78] T. Jiang et al., Solar RRL 4 (2019) 1900467.
[79] R.X. Lin et al., Nat. Energy 4 (2019) 864–873.
[80] H.-C. Wang et al., Small 14 (2018) 1702433.
[81] J. De Roo et al., ACS Nano 10 (2016) 2071–2081.
[82] A. Swarnkar et al., Science 354 (2016) 92–95.
[83] B. Luo et al., Angew. Chem. Int. Ed. 55 (2016) 8864–8868.
[84] D. Di Girolamo et al., Adv. Energy Mater. 10 (2020) 2000310.
[85] R.A. Kerner et al., ACS Energy Lett. 5 (2020) 3352–3356.
[86] S. Reichert et al., Nat. Commun. 11 (2020) 6098.
[87] C. Li et al., Small 13 (2017) 1701711.
[88] Z. Xiao et al., Nat. Mater. 14 (2015) 193–198.
[89] R.A. John et al., Adv. Mater. 30 (2018) 1805454.
[90] R.A. John et al., Adv. Mater. 33 (2021) 2007851.
[91] D.A. Jacobs et al., J. Appl. Phys. 124 (2018) 225702.
[92] A. Zohar et al., J. Phys. Chem. Lett. 7 (2016) 191–197.
[93] F. Fabregat-Santiago et al., ACS Energy Lett. 2 (2017) 2007–2013.
[94] A. Guerrero, J. Bisquert, G. Garcia-Belmonte, Chem. Rev. 121 (2021) 14430–14484.
[95] Y. Lin et al., Nat. Commun. 9 (2018) 4981.
[96] D. Bryant et al., Energy Environ. Sci. 9 (2016) 1655–1660.
[97] N. Aristidou et al., Nat. Commun. 8 (2017) 15218.
[98] W. Li et al., Energy Environ. Sci. 9 (2016) 490–498.
[99] T. Sekimoto et al., ACS Appl. Energy Mater. 2 (2019) 5039–5049.
[100] K. Ji et al., Adv. Opt. Mater. 9 (2021) 2002128.
[101] Z. Xiao et al., Nano Lett. 17 (2017) 6863–6869.
[102] A. Rajagopal et al., Nano Lett. 18 (2018) 3985–3993.
[103] E.T. Hoke et al., Chem. Sci. 6 (2015) 613–617.
[104] C.G. Bischak et al., Nano Lett. 17 (2017) 1028–1033.
[105] S. Draguta et al., Nat. Commun. 8 (2017) 200.
[106] J.P. Correa Baena et al., Energy Environ. Sci. 8 (2015) 2928–2934.
[107] J.-W. Lee et al., Adv. Mater. 26 (2014) 4991–4998.
[108] N. Zhou et al., Small 13 (2017) 1700484.
[109] Y. Zhao et al., Nat. Commun. 9 (2018) 1607.
[110] C. Yi et al., Energy Environ. Sci. 9 (2016) 656–662.
[111] S.-H. Turren-Cruz, A. Hagfeldt, M. Saliba, Science 362 (2018) 449–453.
[112] R.J. Sutton et al., Adv. Energy Mater. 6 (2016) 1502458.
[113] Q. Zhou et al., Adv. Sci. 8 (2021) 2101418.
[114] Y. Hu et al., ACS Energy Lett. 2 (2017) 2219–2227.
[115] A.K. Jena et al., Chem. Mater. 30 (2018) 6668–6674.
[116] S.S. Mali et al., Matter 4 (2021) 635–653.
[117] J. Hu, L. Yan, W. You, Adv. Mater. 30 (2018) 1802041.
[118] W. Fu, H. Chen, A.K.Y. Jen, Mater. Today Nano 14 (2021) 100117.
[119] D.B. Mitzi et al., Nature 369 (1994) 467–469.
[120] T. Ishihara, J. Takahashi, T. Goto, Solid State Commun. 69 (1989) 933–936.
[121] Y. Zhisheng et al., Acta Chim. Sin. 69 (2011) 627–632.
[122] I.C. Smith et al., Angew. Chem. 126 (2014) 11414–11417.
[123] L.N. Quan et al., J. Am. Chem. Soc. 138 (2016) 2649–2655.
[124] H. Tsai et al., Nature 536 (2016) 312–316.
[125] X. Zhang et al., Adv. Energy Mater. 8 (2018) 1702498.
[126] W. Fu et al., ACS Energy Lett. 3 (2018) 2086–2093.
[127] R. Yang et al., Adv. Mater. 30 (2018) e1804771.
[128] J.V. Passarelli et al., J. Am. Chem. Soc. 140 (2018) 7313–7323.
[129] I. Zimmermann, S. Aghazada, M.K. Nazeeruddin, Angew. Chem. Int. Ed. 58 (2019) 1072–1076.
[130] W. Fu et al., Adv. Funct. Mater. 29 (2019) 1900221.
[131] H. Ren et al., Nat. Photonics 14 (2020) 154.
[132] S. Ahmad et al., Joule 3 (2019) 794–806.
[133] Y. Liao et al., J. Am. Chem. Soc. 139 (2017) 6693–6699.
[134] F. Wang et al., Joule 2 (2018) 2732–2743.
[135] Y. Jiang et al., Joule 2 (2018) 1356–1368.

[136] Z. Wang et al., Nat. Energy 2 (2017) 17135.
[137] T. Zhang et al., Sci Adv 3 (2017) e1700841.
[138] S. Tan et al., Angew. Chem. Int. Ed. (2022) e202201300.
[139] K.T. Cho et al., Energy Environ. Sci. 11 (2018) 952–959.
[140] Y. Lin et al., J. Phys. Chem. Lett. 9 (2018) 654–658.
[141] Q.A. Akkerman et al., Nat. Mater. 17 (2018) 394–405.
[142] L. Protesescu et al., Nano Lett. 15 (2015) 3692–3696.
[143] Y. Dong et al., Nat. Nanotechnol. 15 (2020) 668–674.
[144] J. Yuan et al., Joule 4 (2020) 1160–1185.
[145] X. Shen et al., Nano Lett. 19 (2019) 1552–1559.
[146] M. Hao et al., Nat. Energy 5 (2020) 79–88.
[147] Q. Zhao et al., ACS Energy Lett. 5 (2020) 238–247.
[148] J. Xue et al., Joule 2 (2018) 1866–1878.
[149] K. Ji et al., J. Mater. Chem. A 8 (2020) 8104–8112.
[150] P. Tamarat et al., Nat. Mater. 18 (2019) 717–724.
[151] M. Imran et al., J. Am. Chem. Soc. 140 (2018) 2656–2664.
[152] J.A. Vigil et al., ACS Energy Lett. 5 (2020) 2475–2482.
[153] Q. Zhao et al., Nat. Commun. 10 (2019) 2842.
[154] A. Swarnkar, W.J. Mir, A. Nag, ACS Energy Lett. 3 (2018) 286–289.
[155] Q.A. Akkerman et al., ACS Energy Lett. 2 (2017) 2183–2186.
[156] M. Lu et al., Adv. Mater. 30 (2018) 1804691.
[157] A.G. Ricciardulli et al., Nat. Mater. 20 (2021) 1325–1336.
[158] C.K. Chiang et al., Phys. Rev. Lett. 39 (1977) 1098–1101.
[159] H. Min et al., Nature 598 (2021) 444–450.
[160] D. Liu, T.L. Kelly, Nat. Photonics 8 (2014) 133–138.
[161] S.S. Shin et al., Nat. Commun. 6 (2015) 7410.
[162] L. Wang et al., J. Mater. Chem. C 2 (2014) 9087–9090.
[163] J. Liu et al., J. Mater. Chem. A 3 (2015) 11750–11755.
[164] Q. Jiang, X. Zhang, J. You, Small 14 (2018) 1801154.
[165] J. Yang et al., Chem. Mater. 27 (2015) 4229–4236.
[166] Q. Jiang et al., Nat. Energy 2 (2016) 16177.
[167] M. Kim et al., Science 375 (2022) 302–306.
[168] J.J. Yoo et al., Nature 590 (2021) 587–593.
[169] T. Liu et al., Sol. RRL 4 (2020) 2000205.
[170] T. Malinauskas et al., ACS Appl. Mater. Interfaces 7 (2015) 11107–11116.
[171] N.J. Jeon et al., Nat. Energy 3 (2018) 682–689.
[172] J. Liu et al., Energy & Environ. Sci. 7 (2014) 2963–2967.
[173] S. Paek et al., Adv. Mater. (2017) 1606555.
[174] W. Zhou, Z. Wen, P. Gao, Adv. Energy Mater. 8 (2018) 1702512.
[175] Q. Fu et al., ACS Energy Lett. 6 (2021) 1521–1532.
[176] M.M. Tavakoli et al., Energy Environ. Sci. 11 (2018) 3310–3320.
[177] M.J. Jeong et al., Energy Environ. Sci. 14 (2021) 2419–2428.
[178] M.M. Tavakoli et al., Mol. Syst. Des. Eng. 3 (2018) 717–722.
[179] N. Arora et al., Science 358 (2017) 768–771.
[180] H. Zhang et al., Adv. Mater. 29 (2017) 1604984.
[181] S. Ye et al., Nano Lett. 15 (2015) 3723–3728.
[182] H. Zhang et al., ACS Nano 10 (2016) 1503–1511.
[183] M.M. Tavakoli et al., J. Mater. Chem. A 7 (2019) 14753–14760.
[184] W. Chen et al., Science 350 (2015) 944–948.
[185] M.M. Tavakoli et al., Sol. RRL 5 (2021) 2000552.
[186] L. Lanzetta, N. Aristidou, S.A. Haque, J. Phys. Chem. Lett. 11 (2020) 574–585.
[187] S. Yang et al., Science 365 (2019) 473–478.
[188] Y. Chen, H. Zhou, J. Appl. Phys. 128 (2020) 060903.
[189] E. Bi et al., Trends Chem. 3 (2021) 575–588.
[190] Q. Wang et al., Energy Environ. Sci. 10 (2017) 516–522.
[191] J.-H. Yang et al., J. Mater. Chem. A 4 (2016) 13105–13112.
[192] J.H. Wu et al., Adv. Energy Mater. 9 (2019) 1901352.
[193] X. Zheng et al., Nat. Energy 2 (2017) 17102.
[194] N. Li et al., Nat. Energy 4 (2019) 408–415.
[195] M. Abdi-Jalebi et al., Nature 555 (2018) 497–501.
[196] R. Wang et al., Science 366 (2019) 1509–1513.
[197] S. Bai et al., Nature 571 (2019) 245–250.
[198] Y.-H. Lin et al., Science 369 (2020) 96–102.
[199] M. Yang et al., Nat. Commun. 7 (2016) 12305.
[200] M.M. Tavakoli et al., Adv. Energy Mater. 9 (2019) 1802646.
[201] X.P. Zheng et al., Nat. Energy 5 (2020) 131–140.
[202] J. Tong et al., Science 364 (2019) 475–479.
[203] Y. Wang et al., Science 365 (2019) 687–691.
[204] L. Na Quan et al., Nat. Commun. 11 (2020) 170.
[205] J.W. Lee, N.G. Park, Adv. Energy Mater. 10 (2019) 1903249.
[206] L. Shi et al., Science 368 (2020) eaba2412.
[207] S.-H. Jeong et al., Joule 4 (2020) 1206–1235.
[208] J.A. Christians, J.S. Manser, P.V. Kamat, J. Phys. Chem. Lett. 6 (2015) 852–857.
[209] E. Zimmermann et al., APL Mater. 4 (2016) 091901.
[210] E. Zimmermann et al., Nat. Photonics 8 (2014) 669–672.
[211] M.V. Khenkin et al., Nat. Energy 5 (2020) 35–49.
[212] N.A. Luechinger, Dig. Tech. Pap. - SID Int. Symp. 50 (2019) 1172–1175.
[213] Y.-H. Won et al., Nature 575 (2019) 634–638.
[214] H.-M. Kim et al., J. Soc. Inf. Disp. 27 (2019) 347–353.
[215] N.A. Luechinger, Dig. Tech. Pap. - SID Int. Symp. 51 (2020) 1178–1181.
[216] https://www.perovskite-info.com/dscc-perovskite-based-qd-films-lcd-applications-could-enter-market-2022.
[217] L. Protesescu et al., J. Am. Chem. Soc. 138 (2016) 14202–14205.
[218] J. Shamsi et al., Nat. Nanotechnol. 16 (2021) 1164–1168.
[219] Y. Wei, Z. Cheng, J. Lin, Chem. Soc. Rev. 48 (2019) 310–350.
[220] J. Zhou et al., J. Alloy. Compd. 708 (2017) 517–523.
[221] G. Jiang et al., ACS Nano 13 (2019) 10386–10396.
[222] J. Zhou et al., J. Mater. Chem. C 4 (2016) 7601–7606.
[223] Y.H. Song et al., Chem. Eng. J. 313 (2017) 461–465.
[224] H.-C. Wang et al., Angew. Chem. Int. Ed. 55 (2016) 7924–7929.
[225] S. Pathak, Chem. Mater. 27 (2015) 8066–8075.
[226] Y. Wei et al., Adv. Funct. Mater. 27 (2017) 1703535.
[227] T. Xuan et al., Chem. Mater. 31 (2019) 1042–1047.
[228] D. Cortecchia et al., J. Am. Chem. Soc. 139 (2017) 39–42.
[229] I. Neogi et al., ChemSusChem 10 (2017) 3765–3772.
[230] S. Bhaumik et al., Chem. Commun. 52 (2016) 7118–7121.
[231] S.D. Stranks, H.J. Snaith, Nat. Nanotechnol. 10 (2015) 391–402.
[232] L.N. Quan et al., Adv. Mater. 30 (2018) 1801996.
[233] H. Cho et al., Science 350 (2015) 1222–1225.
[234] A.G. Ricciardulli et al., Polymer–perovskite blend light-emitting diodes using a self-compensated heavily doped polymeric anode APL, Mater. 8 (2020).
[235] A.G. Ricciardulli et al., Adv. Electron. Mater. 5 (2019) 1800687.
[236] W. Xu et al., Nat. Photonics 13 (2019) 418–424.
[237] D. Ma et al., Nature 599 (2021) 594–598.
[238] Y.-H. Kim et al., Nat. Photonics 15 (2021) 148–155.
[239] Z. Liu et al., Adv. Mater. 33 (2021) 2103268.
[240] N. Wang et al., Nat. Photonics 10 (2016) 699–704.
[241] J. Song et al., Adv. Mater. 27 (2015) 7162–7167.
[242] D.V. Talapin et al., Chem. Rev. 110 (2010) 389–458.
[243] M.V. Kovalenko, L. Protesescu, M.I. Bodnarchuk, Science 358 (2017) 745–750.
[244] K. Lin et al., Nature 562 (2018) 245–248.
[245] B. Zhao et al., Nat. Photonics 12 (2018) 783–789.
[246] G. Xing et al., Nat. Commun. 8 (2017) 14558.
[247] B. Chen et al., Chem. Soc. Rev. 48 (2019) 3842–3867.
[248] W.K. Bae et al., Nat. Commun. 4 (2013) 2661.
[249] L. Zhang et al., Nat. Commun. 8 (2017) 15640.
[250] Y. Cao et al., Nature 562 (2018) 249–253.
[251] Y. Shang et al., Sci. Adv. 5 (2019) eaaw8072.
[252] O.R. Yamilova et al., J. Phys. Chem. Lett. 11 (2019) 221–228.
[253] Y. Yuan et al., Adv. Energy Mater. 5 (2015) 1500615.
[254] H.J. Jung et al., Adv. Mater. 30 (2018) 1802769.
[255] G.F. Samu et al., J. Am. Chem. Soc. 141 (2019) 10812–10820.
[256] L. Zhao et al., ACS Energy Lett. 1 (2016) 595–602.
[257] A. Kirakosyan et al., J. Phys. Chem. Lett. 10 (2019) 4222–4228.
[258] S.T. Birkhold et al., ACS Energy Lett. 3 (2018) 1279–1286.
[259] Z. Xiao et al., Nat. Photonics 11 (2017) 108–115.
[260] C. Kuang et al., Joule 5 (2021) 618–630.
[261] H. Kim et al., Nat. Commun. 9 (2018) 4893.
[262] M. Anaya et al., Nat. Photonics 13 (2019) 818–821.
[263] X.-K. Liu et al., Nat. Mater. 20 (2021) 10–21.
[264] S. Yakunin et al., Nat. Photonics 9 (2015) 444–449.
[265] H. Wei, J. Huang, Nat. Commun. 10 (2019) 1066.
[266] S. Yakunin et al., Nat. Photonics 10 (2016) 585–589.
[267] O. Nazarenko et al., NPG Asia Mater. 9 (2017). e373–e373.
[268] H. Wei et al., Nat. Mater. 16 (2017) 826–833.
[269] Y. He et al., Nat. Commun. 9 (2018) 1609.
[270] X.Y. Chin et al., Nat. Commun. 6 (2015) 7383.
[271] S.P. Senanayak et al., Sci. Adv. 3 (2017) e1601935.
[272] H.P. Kim et al., Nanoscale 12 (2020) 7641–7650.
[273] S.P. Senanayak et al., Sci. Adv. 6 (2020) eaaz4948.
[274] B. Jeong et al., Adv. Mater. 33 (2021) 2100486.
[275] D.B. Strukov et al., Nature 453 (2008) 80–83.
[276] R.A. John et al., Nat. Commun. 12 (2021) 3681.
[277] P.C. Harikesh et al., MRS Bull. 45 (2020) 641–648.
[278] Y. Wang et al., Adv. Mater. 30 (2018) 1800327.
[279] S. Lee et al., ACS Appl. Mater. Interfaces 12 (2020) 17039–17045.

[280] Z. Xiao, J. Huang, Adv. Electron. Mater. 2 (2016) 1600100.
[281] W. Xu et al., Adv. Mater. 28 (2016) 5916–5922.
[282] Z. Zhu et al., J. Mater. Chem. C 6 (2018) 10121–10137.
[283] C. Bao et al., Chem. Commun. 51 (2015) 15426–15429.
[284] Y. Zhao, K. Zhu, Chem. Commun. 50 (2014) 1605–1607.
[285] L. Xie et al., Front. Chem. 9 (2021) 682006.
[286] K. Ren et al., J. Mater. Chem. C 5 (2017) 2504–2508.
[287] W. Xu et al., J. Mater. Chem. C 4 (2016) 9651–9655.
[288] G. Huang et al., Adv. Mater. 29 (2017) 1700095.
[289] Y. Huang et al., Microchim. Acta 184 (2017) 3513–3519.
[290] X. Sheng et al., Adv. Mater. 29 (2017) 1700150.
[291] M. Aamir et al., Mater. Lett. 183 (2016) 135–138.
[292] M. Aamir et al., Eur. J. Inorg. Chem. 2017 (2017) 3755–3760.